PERGAMON

International Journal of Solids and Structures 40 (2003) 4257–4279

INTERNATIONAL JOURNAL OF SOLIDS and STRUCTURES

www.elsevier.com/locate/ijsolstr

A spiral model for bending of non-linearly pretwisted helicoidal structures with lateral loading

C.W. Lim *

Department of Building and Construction, City University of Hong Kong, Tat Chee Avenue, Kowloon, Hong Kong

Received 15 February 2003

Abstract

The paper presents a new approach in the bending analysis of helicoidal structures with a large non-linear pretwist and an external lateral loading. It also addresses the issue as to what extent the linearized twisting curvature is applicable in the analysis of pretwisted plates. Employing a non-linear helicoidal model and a natural orthogonal coordinate system, the large non-linear pretwist is formulated and the energy stored in a distorted helicoid subjected to an external pressure normal to the helicoid axis is derived. By integrating the internal strain energy and external pressure work over the helicoidal domain, a non-homogeneous system of equations is presented and numerical solutions are obtained. Significant structural responses such as deformation components and resultant, the effects of width and thickness of helicoid on bending are analyzed and discussed. The analysis can be extended to other areas of interest such as turbomachinery blades, drilling structures, motors in micro-electro-mechanical systems and also DNA biomechanics.

Keywords: Loading; Plates; Strain

1. Introduction

Helicoidal structures are essential components in many engineering applications such as turbomachinery blades and drilling structures. Although they belong to the same family of helicoidal structures, the former has attracted intensive research in mechanical engineering (Reissner, 1954, 1959; Maunder and Reissner, 1957; Knowles and Reissner, 1959; O'Mathuna, 1963; Wan, 1967, 1968, 1969a,b, 1970, 1990; Reissner and Wan, 1968; Mallett and Wan, 1971, 1973; Leissa, 1973, 1980, 1981; Leissa et al., 1982, 1984; Leissa and Ewing, 1983; Rao, 1973, 1977, 1980, 1983, 1987, 1991) while the latter is a subject of rock mechanics interested in civil, mining and petroleum engineering disciplines (Selvam and Sujatha, 1995; Christoforou and Yigit, 1997; Challamel, 2000). With the advent of modern technology in micro-electro-mechanical-systems (MEMS), helicoidal structures find many new uses in minute motor and turbine systems integrated into electronic circuits.

* Tel.: +852-2788-7285; fax: +852-2788-7612.
E-mail address: bccwlim@cityu.edu.hk (C.W. Lim).

0020-7683/03/$ - see front matter
doi:10.1016/S0020-7683(03)00198-7

The separation of research in helicoidal structures by two different groups of researchers is mainly due to direct relevancy in their fields of engineering applications. The analytical, numerical and experimental solutions for turbomachinery blades are abundant (Leissa et al., 1984; Kielb et al., 1985; MacBain et al., 1985) while established research in dynamics of drilling structures is limited to simple models and empirical results because of the complexity in modelling and operating conditions. The reason is obvious. In modelling and analysis, a turbomachinery blade can be modelled as a beam (Rao and Carnegie, 1970; Rao, 1991; Leung, 1991; Leung and Chan, 1997), a plate (Wan, 1969b; Reissner and Wan, 1971; Leissa et al., 1984; Rao, 1991; Liew and Lim, 1994a; Lim and Liew, 1995a) or a shell with a small linear pretwist (Leissa et al., 1982; Leissa and Ewing, 1983; Lee et al., 1984; Liew and Lim, 1994b; Liew et al., 1994, 1995; Lim and Liew, 1995b) but such assumption is not valid for drill. Analytical and numerical solutions for turbomachinery blades could be obtained quite directly by solving the governing homogeneous or eigenvalue system.

In turbomachinery blade analysis, the beam model is accurate for slender blades. For blades with a small aspect ratio, the plate and shell models are more appropriate. Shell models are preferable to plate models because the effect of surface curvature is considered. The shallow cylindrical shell model has been applied by Leissa and his associates to study the vibration of blades with uniform (Leissa et al., 1982; Leissa and Ewing, 1983) or variable thickness (Lee et al., 1984). A similar analysis has also been undertaken by Liew and Lim (1994b) for cylindrical shells with generally varying thickness. One major deficiency of the cylindrical shallow shell model, however, is the constant chordwise curvature. A better model of an actual turbomachinery blade should feature a shallow shell with not only non-uniform planform but also variable chordwise curvature. Thus an open conical shell model is more appropriate. The vibration of open conical shells has been reported respectively for untwisted shells with uniform thickness (Lim and Liew, 1995b), pretwisted shells with uniform thickness (Liew et al., 1994), and pretwisted shells with variable thickness (Liew et al., 1995).

Despite the intensive research on turbomachinery blades as describe above, to the author's knowledge, most of the publications assume linear pretwist and are valid only for a small angle of pretwist, presumably less than 30°. In some of the publications, numerical solutions were presented for blades of up to 45° of angle of pretwist. These results are thus unreliable and the models cannot be applied to analyze structural dynamics of drills as drills are helicoidal structures with highly non-linear pretwist. Among some analyses which consider large non-linear pretwist of plates and helicoidal shells with and without side-force are Reissner (1954, 1959), Maunder and Reissner (1957), Knowles and Reissner (1959), O'Mathuna (1963), Wan (1967, 1968, 1969a,b, 1970, 1990), Reissner and Wan (1968), Mallett and Wan (1971, 1973) analyzing the axial extension, torsion, rotationally symmetric shearing, bending and spirally sinusoidal stress distribution. Besides, Walker (1978) considered the vibration of fan blades, Tsuiji et al. (1994a,b) presented formulation for free vibration of curved, pretwisted thin plates using a non-orthogonal coordinate system and Mockensturm and Mote (2001) analyzed the response of twisted plates with fixed support separation. Although significant solutions were presented for helicoidal structures with large angle of pretwist, no solutions are available for bending of such structures in the presence of an external lateral surface loading.

In this paper, it is intended to present a new approach and numerical solutions for bending analysis of helicoidal drilling structures, i.e. structures with highly non-linear pretwist, subject to an external lateral loading. It also discussed the extent of applicability of linearized twisting curvature in the analysis of pretwisted plates. With reference to a natural orthogonal coordinate system, the non-linear pretwist is formulated and the energy stored in a distorted drill model subjected to constant transverse pressure is derived based on the shell theory of Goldenveizer (1961) and Novozhilov (1964). By integrating the internal strain energy and external pressure work over the drill domain, a non-homogeneous system of equations is presented and numerical solutions are obtained. Significant structural responses such as deformation components, bending resultants and the effects of width and thickness of helicoid are analyzed and dis-

cussed. The analysis can be extended to other areas of interest such as applications of blades and motors in MEMS and also on biomechanics if the non-Newtonian fluid lateral loading is taken into consideration.

2. Helicoidal model with non-linear pretwist and formulation of strains

The geometry of a helix and a helicoid with length a, radius R, width b and projected angle of pretwist θ_0 (at a) are shown in Figs. 1 and 2. The helicoidal structure is subject to a lateral load $\boldsymbol{q}$. For such a helicoid we impose a condition of $b < R$. A curvilinear coordinate system, perpendicular and tangential to the helix and lying in the osculating plane $(\boldsymbol{r}, \partial\boldsymbol{r}/\partial\theta)$, is adopted. With the binormal vector to the helix $\boldsymbol{b}$, it forms an orthogonal coordinate system $(\boldsymbol{r}, \partial\boldsymbol{r}/\partial\theta, \boldsymbol{b})$, and its transformation with respect to the Cartesian system $(\boldsymbol{i}, \boldsymbol{j}, \boldsymbol{k})$ is

$$\boldsymbol{r} = r(\cos\theta\boldsymbol{i} + \sin\theta\boldsymbol{j}) + \frac{\theta}{\varphi}\boldsymbol{k} \tag{1}$$

where $\varphi = \theta_0/a$ is the rate of change of θ along the z-axis, or the rate of pretwist. For this curvilinear coordinate system, the Lamé parameters or coefficients of the first quadratic form can be derived as $h_r = 1$, $h_\theta = (1/\varphi)\sqrt{1 + r^2\varphi^2}$ and the base vectors are

$$\begin{aligned}
\boldsymbol{e}_r &= \cos\theta\boldsymbol{i} + \sin\theta\boldsymbol{j} \\
\boldsymbol{e}_\theta &= \frac{1}{h_\theta}\left[-r\sin\theta\boldsymbol{i} + r\cos\theta\boldsymbol{j} + \frac{1}{\varphi}\boldsymbol{k}\right] \\
\boldsymbol{e}_b &= \frac{1}{\varphi h_\theta}[\sin\theta\boldsymbol{i} - \cos\theta\boldsymbol{j} + r\varphi\boldsymbol{k}]
\end{aligned} \tag{2a–c}$$

Deriving from the theory of surfaces (Young, 1993), a helix (Fig. 1) has an infinite radius of curvature with respect to the coordinates (r, θ), whereas the radius of twist (or torsion of the space curve $\boldsymbol{r}$) is finite as (Lim, 1999a,b)

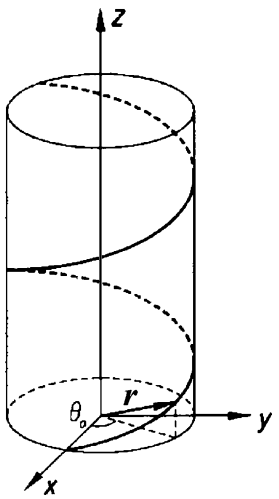

Fig. 1. Geometry of a helix.

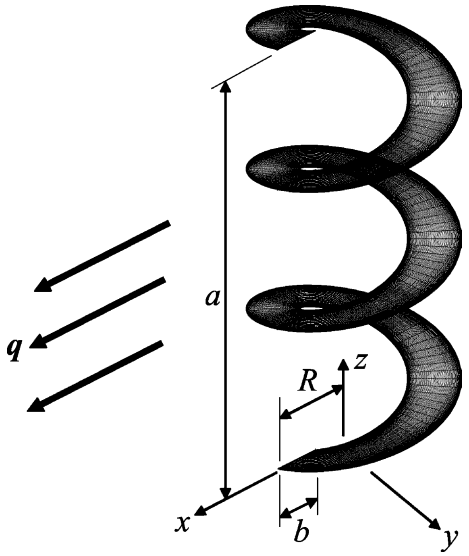

Fig. 2. Geometry of a helicoidal structure.

$$\frac{1}{R_r}=0;\quad \frac{1}{R_\theta}=0;\quad \frac{1}{R_{r\theta}}=-\frac{\varphi}{1+r^2\varphi^2}=-\frac{1}{\varphi h_\theta^2} \tag{3a–c}$$

where R_r and R_θ are the radius of curvatures in the r- and θ-directions, respectively, and $R_{r\theta}$ is the radius of twist. The twisting curvature derived in Eq. (3c) is non-linear and, therefore, it accommodates a surface with an arbitrarily large twisting curvature instead of the linearized twisting curvature (Leissa et al., 1982, 1984; Leissa and Ewing, 1983; Lee et al., 1984; Liew and Lim, 1994a,b; Liew et al., 1994, 1995; Lim and Liew, 1995a,b) which is only valid for a small angle of pretwist.

Let $\boldsymbol{u}(r,\theta)$ be the displacement vector composing of u_r, u_θ in the osculating plane and u_b in the binormal direction, then the linear normal strains, shear strains, changes of curvature and twist can be derived based on the shell theory of Goldenveizer (1961) and Novozhilov (1964) as

$$\varepsilon_{rr}=\frac{\partial u_r}{\partial r};\quad \varepsilon_{\theta\theta}=\frac{1}{h_\theta}\frac{\partial u_\theta}{\partial\theta}+\frac{ru_r}{h_\theta^2};\quad \gamma_{r\theta}=\frac{\partial u_\theta}{\partial r}-\frac{ru_\theta}{h_\theta^2}+\frac{1}{h_\theta}\frac{\partial u_r}{\partial\theta}-\frac{2u_b}{\varphi h_\theta^2} \tag{4a–c}$$

$$\kappa_{rr}=-\frac{3}{2\varphi h_\theta^2}\frac{\partial u_\theta}{\partial r}+\frac{3ru_\theta}{2\varphi h_\theta^4}-\frac{\partial^2 u_b}{\partial r^2}+\frac{1}{2\varphi h_\theta^3}\frac{\partial u_r}{\partial\theta} \tag{4d}$$

$$\kappa_{\theta\theta}=-\frac{3}{2\varphi h_\theta^3}\frac{\partial u_r}{\partial\theta}-\frac{1}{h_\theta^2}\frac{\partial^2 u_b}{\partial\theta^2}-\frac{ru_\theta}{2\varphi h_\theta^4}-\frac{r}{h_\theta^2}\frac{\partial u_b}{\partial r}+\frac{1}{2\varphi h_\theta^2}\frac{\partial u_\theta}{\partial r} \tag{4e}$$

$$\tau_{r\theta}=\frac{1}{h_\theta}\frac{\partial^2 u_b}{\partial r\partial\theta}+\frac{r}{h_\theta^3}\frac{\partial u_b}{\partial\theta}-\frac{1}{\varphi h_\theta^2}\frac{\partial u_r}{\partial r}-\frac{1}{\varphi h_\theta^3}\frac{\partial u_\theta}{\partial\theta}+\frac{ru_r}{\varphi h_\theta^4} \tag{4f}$$

The strain expressions above deviate slightly from the expressions of Wan (1967, 1968) and Reissner and Wan (1968) which may be due to different shell theories adopted.

3. Formulation of energy, work and a non-homogeneous system

During bending, the strain energy for a helicoidal structure with a constant thickness h can be expressed as

$$\begin{aligned} U &= U_{\mathrm{s}} + U_{\mathrm{b}} \\ &= \frac{6D}{h^2}\int\int_A \left[\varepsilon_{rr}^2 + \varepsilon_{\theta\theta}^2 + 2\nu\varepsilon_{rr}\varepsilon_{\theta\theta} + \frac{1-\nu}{2}\gamma_{r\theta}^2\right] h_\theta \,\mathrm{d}r\,\mathrm{d}\theta \\ &\quad + \frac{D}{2}\int\int_A \left[\kappa_{rr}^2 + \kappa_{\theta\theta}^2 + 2\nu\kappa_{rr}\kappa_{\theta\theta} + 2(1-\nu)\tau_{r\theta}^2\right] h_\theta \,\mathrm{d}r\,\mathrm{d}\theta \end{aligned} \tag{5}$$

where $D = Eh^3/12(1-\nu^2)$ is the flexural rigidity, E is the Young's modulus and ν is the Poisson ratio. The first and second integrals in Eq. (5) correspond to the stretching strain energy, U_{s}, and bending strain energy, U_{b}, respectively. Equations for varying thickness $h(r,\theta)$ can be reformulated accordingly, by retaining $h^3(r,\theta)$ in the domain integrals for strain energy in Eq. (5).

The work done due to external loading is

$$W = \int\int_A \boldsymbol{q}(r,\theta)\cdot\boldsymbol{u}(r,\theta) h_\theta \,\mathrm{d}r\,\mathrm{d}\theta \tag{6}$$

where $\boldsymbol{q}(r,\theta)$ is the loading distribution over domain A. Assuming the loading normal to helicoid axis is along the positive x-direction (Fig. 2) and be represented by $\boldsymbol{q} = q\boldsymbol{i}$. As the helicoid is assumed infinitely long, it is possible to analyze only *one unit* (360°) of the repeating helicoid. Decomposing $\boldsymbol{q} = q\boldsymbol{i}$ in the orthogonal coordinate system $(\boldsymbol{r}, \partial\boldsymbol{r}/\partial\theta, \boldsymbol{b})$ yields

$$\boldsymbol{q} = q\cos\theta\boldsymbol{e}_r - \frac{qr\sin\theta}{h_\theta}\boldsymbol{e}_\theta + \frac{q\sin\theta}{\varphi h_\theta}\boldsymbol{e}_b \tag{7}$$

Substituting Eq. (7) into Eq. (6) yields the work done on the helicoid as

$$W = q\int\int_A \left[h_\theta\cos\theta u_r - r\sin\theta u_\theta + \frac{\sin\theta}{\varphi}u_b\right]\mathrm{d}r\,\mathrm{d}\theta \tag{8}$$

For brevity and generality, a set of dimensionless coordinate system and dimensionless parameters are defined as

$$\bar{r} = \frac{r}{R};\quad \overline{\theta} = \frac{\theta}{\theta_0};\quad \overline{\varphi} = R\varphi;\quad \bar{h}_\theta = \frac{h_\theta}{R};\quad \bar{u}_r = \frac{u_r}{R};\quad \bar{u}_\theta = \frac{u_\theta}{R};\quad \bar{u}_b = \frac{u_b}{R} \tag{9a–g}$$

Using these non-dimensional scheme and substituting expressions in Eqs. (4a–f) into the equations for stretching strain energy and bending strain energy in Eq. (5) yield

$$\begin{aligned} U_{\mathrm{s}} = \frac{6D}{h^2}\int\int_{\bar{A}} \Bigg\{ & \theta_0\bar{h}_\theta\left(\frac{\partial\bar{u}_r}{\partial\bar{r}}\right)^2 + \frac{1}{\bar{h}_\theta}\left(\frac{\partial\bar{u}_\theta}{\partial\overline{\theta}}\right)^2 + \frac{2\bar{r}}{\bar{h}_\theta^2}\bar{u}_r\frac{\partial\bar{u}_\theta}{\partial\overline{\theta}} + \frac{\theta_0\bar{r}^2}{\bar{h}_\theta^3}\bar{u}_r^2 + 2\nu\frac{\partial\bar{u}_r}{\partial\bar{r}}\left[\frac{\partial\bar{u}_\theta}{\partial\overline{\theta}} + \frac{\theta_0\bar{r}}{\bar{h}_\theta}\bar{u}_r\right] \\ & + \frac{1-\nu}{2}\left[\theta_0\bar{h}_\theta\left(\frac{\partial\bar{u}_\theta}{\partial\bar{r}}\right)^2 - \frac{2\theta_0\bar{r}}{\bar{h}_\theta}\bar{u}_\theta\frac{\partial\bar{u}_\theta}{\partial\bar{r}} + 2\frac{\partial\bar{u}_r}{\partial\overline{\theta}}\frac{\partial\bar{u}_\theta}{\partial\bar{r}} - \frac{4\theta_0}{\overline{\varphi}\bar{h}_\theta}\frac{\partial\bar{u}_\theta}{\partial\bar{r}}\bar{u}_b + \frac{\theta_0\bar{r}^2}{\bar{h}_\theta^3}\bar{u}_\theta^2 - \frac{2\bar{r}}{\bar{h}_\theta^2}\frac{\partial\bar{u}_r}{\partial\overline{\theta}}u_\theta \right. \\ & \left. + \frac{4\theta_0\bar{r}}{\overline{\varphi}\bar{h}_\theta^3}\bar{u}_\theta\bar{u}_b + \frac{1}{\theta_0\bar{h}_\theta}\left(\frac{\partial\bar{u}_r}{\partial\overline{\theta}}\right)^2 - \frac{4}{\overline{\varphi}\bar{h}_\theta^2}\frac{\partial\bar{u}_r}{\partial\overline{\theta}}\bar{u}_b + \frac{4\theta_0}{\overline{\varphi}^2\bar{h}_\theta^3}\bar{u}_b^2\right]\Bigg\}\mathrm{d}\bar{r}\,\mathrm{d}\overline{\theta} \end{aligned} \tag{10}$$

and

$$U_{\mathrm{b}} = \frac{D}{2}\int\int_{\bar{A}}\left\{\frac{5-3v}{2\theta_0\overline{\varphi}^2\bar{h}_\theta^5}\left(\frac{\partial\bar{u}_r}{\partial\overline{\theta}}\right)^2+\frac{(3-5v)\bar{r}}{\overline{\varphi}^2\bar{h}_\theta^6}\frac{\partial\bar{u}_r}{\partial\overline{\theta}}\bar{u}_\theta-\frac{3-5v}{\overline{\varphi}^2\bar{h}_\theta^4}\frac{\partial\bar{u}_r}{\partial\overline{\theta}}\frac{\partial\bar{u}_\theta}{\partial\bar{r}}+\frac{(3-v)\bar{r}}{\overline{\varphi}\bar{h}_\theta^4}\frac{\partial\bar{u}_r}{\partial\overline{\theta}}\frac{\partial\bar{u}_b}{\partial\bar{r}}\right.$$

$$-\frac{1-3v}{\overline{\varphi}\bar{h}_\theta^2}\frac{\partial\bar{u}_r}{\partial\overline{\theta}}\frac{\partial^2\bar{u}_b}{\partial\bar{r}^2}+\frac{3-v}{\theta_0\overline{\varphi}\bar{h}_\theta^4}\frac{\partial\bar{u}_r}{\partial\overline{\theta}}\frac{\partial^2\bar{u}_b}{\partial\overline{\theta}^2}+\frac{(5-3v)\theta_0\bar{r}^2}{2\overline{\varphi}^2\bar{h}_\theta^7}\bar{u}_\theta^2-\frac{(5-3v)\theta_0\bar{r}}{\overline{\varphi}^2\bar{h}_\theta^5}\bar{u}_\theta\frac{\partial\bar{u}_\theta}{\partial\bar{r}}$$

$$+\frac{(1-3v)\theta_0\bar{r}^2}{\overline{\varphi}\bar{h}_\theta^5}\bar{u}_\theta\frac{\partial\bar{u}_b}{\partial\bar{r}}-\frac{(3-v)\theta_0\bar{r}}{\overline{\varphi}\bar{h}_\theta^3}\bar{u}_\theta\frac{\partial^2\bar{u}_b}{\partial\bar{r}^2}+\frac{(1-3v)\bar{r}}{\theta_0\overline{\varphi}\bar{h}_\theta^5}\bar{u}_\theta\frac{\partial^2\bar{u}_b}{\partial\overline{\theta}^2}-\frac{(5-3v)\theta_0}{2\overline{\varphi}^2\bar{h}_\theta^3}\left(\frac{\partial\bar{u}_\theta}{\partial\bar{r}}\right)^2$$

$$+\frac{(1-3v)\theta_0\bar{r}}{\overline{\varphi}\bar{h}_\theta^3}\frac{\partial\bar{u}_\theta}{\partial\bar{r}}\frac{\partial\bar{u}_b}{\partial\bar{r}}+\frac{(3-v)\theta_0}{\overline{\varphi}\bar{h}_\theta}\frac{\partial\bar{u}_\theta}{\partial\bar{r}}\frac{\partial^2\bar{u}_b}{\partial\bar{r}^2}-\frac{1-3v}{\theta_0\overline{\varphi}\bar{h}_\theta^3}\frac{\partial\bar{u}_\theta}{\partial\bar{r}}\frac{\partial^2\bar{u}_b}{\partial\overline{\theta}^2}-\frac{\theta_0\bar{r}^2}{\bar{h}_\theta^3}\left(\frac{\partial\bar{u}_b}{\partial\bar{r}}\right)^2$$

$$+\frac{2v\theta_0\bar{r}}{\bar{h}_\theta}\frac{\partial\bar{u}_b}{\partial\bar{r}}\frac{\partial^2\bar{u}_b}{\partial\bar{r}^2}+\frac{2\bar{r}}{\theta_0\bar{h}_\theta^3}\frac{\partial\bar{u}_b}{\partial\bar{r}}\frac{\partial^2\bar{u}_b}{\partial\overline{\theta}^2}+\theta_0\bar{h}_\theta\left(\frac{\partial^2\bar{u}_b}{\partial\bar{r}^2}\right)^2+\frac{2v}{\theta_0\bar{h}_\theta}\frac{\partial^2\bar{u}_b}{\partial\bar{r}^2}\frac{\partial^2\bar{u}_b}{\partial\overline{\theta}^2}+\frac{1}{\theta_0^3\bar{h}_\theta^3}\left(\frac{\partial^2\bar{u}_b}{\partial\overline{\theta}^2}\right)^2$$

$$+\frac{2(1-v)}{\bar{h}_\theta}\left[\frac{1}{\theta_0}\left(\frac{\partial^2\bar{u}_b}{\partial\bar{r}\partial\overline{\theta}}\right)^2-\frac{2\bar{r}}{\theta_0\bar{h}_\theta^2}\frac{\partial\bar{u}_b}{\partial\overline{\theta}}\frac{\partial^2\bar{u}_b}{\partial\bar{r}\partial\overline{\theta}}+\frac{2}{\overline{\varphi}\bar{h}_\theta}\frac{\partial\bar{u}_r}{\partial\bar{r}}\frac{\partial^2\bar{u}_b}{\partial\bar{r}\partial\overline{\theta}}+\frac{2}{\theta_0\overline{\varphi}\bar{h}_\theta^2}\frac{\partial\bar{u}_\theta}{\partial\overline{\theta}}\frac{\partial^2\bar{u}_b}{\partial\bar{r}\partial\overline{\theta}}-\frac{2\bar{r}}{\overline{\varphi}\bar{h}_\theta^3}\bar{u}_r\frac{\partial^2\bar{u}_b}{\partial\bar{r}\partial\overline{\theta}}\right.$$

$$+\frac{\bar{r}^2}{\theta_0\bar{h}_\theta^4}\left(\frac{\partial\bar{u}_b}{\partial\overline{\theta}}\right)^2-\frac{2\bar{r}}{\overline{\varphi}\bar{h}_\theta^3}\frac{\partial\bar{u}_r}{\partial\bar{r}}\frac{\partial\bar{u}_b}{\partial\overline{\theta}}-\frac{2\bar{r}}{\theta_0\overline{\varphi}\bar{h}_\theta^4}\frac{\partial\bar{u}_\theta}{\partial\overline{\theta}}\frac{\partial\bar{u}_b}{\partial\overline{\theta}}+\frac{2\bar{r}^2}{\overline{\varphi}\bar{h}_\theta^5}\bar{u}_r\frac{\partial\bar{u}_b}{\partial\overline{\theta}}+\frac{\theta_0}{\overline{\varphi}^2\bar{h}_\theta^2}\left(\frac{\partial\bar{u}_r}{\partial\bar{r}}\right)^2+\frac{2}{\overline{\varphi}^2\bar{h}_\theta^3}\frac{\partial\bar{u}_r}{\partial\bar{r}}\frac{\partial\bar{u}_\theta}{\partial\overline{\theta}}$$

$$\left.\left.-\frac{2\theta_0\bar{r}}{\overline{\varphi}^2\bar{h}_\theta^4}\bar{u}_r\frac{\partial\bar{u}_r}{\partial\bar{r}}+\frac{1}{\theta_0\overline{\varphi}^2\bar{h}_\theta^4}\left(\frac{\partial\bar{u}_\theta}{\partial\overline{\theta}}\right)^2-\frac{2\bar{r}}{\overline{\varphi}^2\bar{h}_\theta^5}\bar{u}_r\frac{\partial\bar{u}_\theta}{\partial\overline{\theta}}+\frac{\theta_0\bar{r}^2}{\overline{\varphi}^2\bar{h}_\theta^6}\bar{u}_r^2\right]\right\}\mathrm{d}\bar{r}\,\mathrm{d}\overline{\theta} \tag{11}$$

which involve the integration over the normalized domain $\overline{A}$. In terms of these dimensionless terms, the external work can be expressed as

$$W = qR^3\theta_0\int\int_{\bar{A}}\left[\bar{h}_\theta\cos\theta\bar{u}_r - r\sin\theta\bar{u}_\theta+\frac{\sin\theta}{\varphi}\bar{u}_b\right]\mathrm{d}\bar{r}\,\mathrm{d}\overline{\theta} \tag{12}$$

The dimensionless displacement components $(\bar{u}_r,\bar{u}_\theta,\bar{u}_b)$ may be represented as a general two-dimensional polynomial series as

$$\bar{u}_r=\sum_{i=1}^{m}C_r^i\phi_r^i(\bar{r},\overline{\theta});\quad \bar{u}_\theta=\sum_{i=1}^{m}C_\theta^i\phi_\theta^i(\bar{r},\overline{\theta});\quad \bar{u}_b=\sum_{i=1}^{m}C_b^i\phi_b^i(\bar{r},\overline{\theta}) \tag{13a–c}$$

where C_r^i, C_θ^i, C_b^i are coefficients and ϕ_r^i, ϕ_θ^i, ϕ_b^i are admissible shape functions of the i-term. The admissible shape functions can be represented by truncated two-dimensional polynomial series to be defined in due course.

In accordance with the Ritz principle, an energy functional can be defined as

$$F = U - W \tag{14}$$

which can be minimized with respect to the coefficients as

$$\frac{\partial F}{\partial C_r^i}=0;\quad \frac{\partial F}{\partial C_\theta^i}=0;\quad \frac{\partial F}{\partial C_b^i}=0 \tag{15}$$

to yield a system of non-homogeneous equations as

$$[\boldsymbol{K}]\{\boldsymbol{C}\}-\{\boldsymbol{Q}\}=0 \tag{16}$$

where

$$[\boldsymbol{K}] = \begin{bmatrix} \boldsymbol{K}_{rr} & \boldsymbol{K}_{r\theta} & \boldsymbol{K}_{rb} \\ & \boldsymbol{K}_{\theta\theta} & \boldsymbol{K}_{\theta b} \\ \text{sym} & & \boldsymbol{K}_{bb} \end{bmatrix}; \quad \{\boldsymbol{C}\} = \begin{Bmatrix} \boldsymbol{C}_r \\ \boldsymbol{C}_\theta \\ \boldsymbol{C}_b \end{Bmatrix}; \quad \{\boldsymbol{Q}\} = \begin{Bmatrix} \boldsymbol{Q}_r \\ \boldsymbol{Q}_\theta \\ \boldsymbol{Q}_b \end{Bmatrix} \tag{17a–c}$$

are the stiffness matrix, displacement coefficient vector and external loading vector, respectively. Elements of the stiffness sub-matrices can be derived as

$$\begin{aligned} \boldsymbol{K}_{rr}^{ij} = {} & \frac{12R^2}{h^2}\left[I_{rr}^{ij(1010;0,1)} + I_{rr}^{ij(0000;2,-3)} + v\left(I_{rr}^{ij(0010;0,-1)} + I_{rr}^{ij(1000;0,1)}\right) + \frac{1-v}{2\theta_0^2} I_{rr}^{ij(0101;0,-1)}\right] \\ & + \frac{5-3v}{2\overline{\varphi}^2\theta_0^2} I_{rr}^{ij(0101;0,-5)} + \frac{2(1-v)}{\overline{\varphi}^2}\left(I_{rr}^{ij(1010;0,-3)} - I_{rr}^{ij(0010;1,-5)} - I_{rr}^{ij(1000;1,-5)} - I_{rr}^{ij(0000;2,-7)}\right) \end{aligned} \tag{18a}$$

$$\begin{aligned} \boldsymbol{K}_{r\theta}^{ij} = {} & \frac{12R^2}{h^2\theta_0}\left[I_{r\theta}^{ij(0001;1,-2)} + vI_{r\theta}^{ij(1001;0,0)} + \frac{1-v}{2}\left(I_{r\theta}^{ij(0110;0,0)} + I_{r\theta}^{ij(0100;1,-2)}\right)\right] \\ & + \frac{3-5v}{2\overline{\varphi}^2\theta_0}\left(I_{r\theta}^{ij(0100;1,-6)} - I_{r\theta}^{ij(0100;1,-4)}\right) + \frac{2(1-v)}{\overline{\varphi}^2\theta_0}\left(I_{r\theta}^{ij(1001;1,-4)} - I_{r\theta}^{ij(0001;1,-6)}\right) \end{aligned} \tag{18b}$$

$$\begin{aligned} \boldsymbol{K}_{rb}^{ij} = {} & -\frac{12R^2(1-v)}{h^2\overline{\varphi}\theta_0} I_{rb}^{ij(0100;0,-2)} + \frac{3-v}{2\overline{\varphi}\theta_0}\left(I_{rb}^{ij(0110;1,-4)} + I_{rb}^{ij(0102;0,-4)}\right) - \frac{1-3v}{2\overline{\varphi}\theta_0} I_{rb}^{ij(0120;0,-2)} \\ & + \frac{2(1-v)}{\overline{\varphi}\theta_0}\left(I_{rb}^{ij(1011;0,-2)} - I_{rb}^{ij(0011;1,-4)} - I_{rb}^{ij(1001;1,-4)} - I_{rb}^{ij(0001;2,-6)}\right) \end{aligned} \tag{18c}$$

$$\begin{aligned} \boldsymbol{K}_{\theta\theta}^{ij} = {} & \frac{12R^2}{h^2}\left[\frac{1}{\theta_0} I_{\theta\theta}^{ij(0101;1,-1)} + \frac{1-v}{2}\left(I_{\theta\theta}^{ij(1010;0,1)} - I_{\theta\theta}^{ij(0010;1,-1)} - I_{\theta\theta}^{ij(1000;1,-1)} + I_{\theta\theta}^{ij(0000;2,-3)}\right)\right] \\ & + \frac{5-3v}{2\overline{\varphi}^2}\left(I_{\theta\theta}^{ij(1010;2,-7)} - I_{\theta\theta}^{ij(0010;1,-5)} - I_{\theta\theta}^{ij(1000;1,-5)} - I_{\theta\theta}^{ij(1010;0,-3)}\right) + \frac{2(1-v)}{\overline{\varphi}^2\theta_0^2} I_{\theta\theta}^{ij(0101;0,-5)} \end{aligned} \tag{18d}$$

$$\begin{aligned} \boldsymbol{K}_{\theta b}^{ij} = {} & \frac{12R^2(1-v)}{h^2\overline{\varphi}}\left(I_{\theta b}^{ij(0000;1,-3)} - I_{\theta b}^{ij(1000;0,-1)}\right) + \frac{1-3v}{2\overline{\varphi}}\left(I_{\theta b}^{ij(0010;2,-5)} - I_{\theta b}^{ij(1010;1,-3)} + \frac{1}{\theta_0^2} I_{\theta b}^{ij(0002;1,-5)}\right. \\ & \left. - \frac{1}{\theta_0^2} I_{\theta b}^{ij(1002;0,-3)}\right) + \frac{3-v}{2\overline{\varphi}}\left(I_{\theta b}^{ij(1020;0,-1)} - I_{\theta b}^{ij(0020;1,-3)}\right) + \frac{2(1-v)}{\overline{\varphi}\theta_0^2}\left(I_{\theta b}^{ij(0111;0,-3)} - I_{\theta b}^{ij(0101;1,-5)}\right) \end{aligned} \tag{18e}$$

$$\begin{aligned} \boldsymbol{K}_{bb}^{ij} = {} & \frac{24R^2(1-v)}{h^2\overline{\varphi}^2} I_{bb}^{ij(0000;0,-3)} + I_{bb}^{ij(1010;2,-3)} + I_{bb}^{ij(2020;0,1)} + v\left(I_{bb}^{ij(1020;1,-1)} + I_{bb}^{ij(2010;1,-1)}\right) \\ & + \frac{1}{\theta_0^2}\left[I_{bb}^{ij(1002;1,-3)} + I_{bb}^{ij(0210;1,-3)} + v\left(I_{bb}^{ij(2002;0,-1)} + I_{bb}^{ij(0220;0,-1)}\right)\right] + \frac{1}{\theta_0^4} I_{bb}^{ij(0202;0,-3)} \\ & + \frac{2(1-v)}{\theta_0^2}\left(I_{bb}^{ij(1111;0,-1)} - I_{bb}^{ij(0111;1,-3)} - I_{bb}^{ij(1101;1,-3)} + I_{bb}^{ij(0101;2,-5)}\right) \end{aligned} \tag{18f}$$

and elements of the external load vector are

$$\boldsymbol{Q}_r^i = \frac{qR^3}{D}\int\int_{\bar{A}} \bar{h}_\theta \cos\theta \phi_r^i \, \mathrm{d}\bar{r}\,\mathrm{d}\bar{\theta} \tag{19a}$$

$$\boldsymbol{Q}_{\theta}^{i} = -\frac{qR^3}{D}\int\int_{\overline{A}} \bar{r}_{\theta}\sin\theta\phi_{\theta}^{i}\,\mathrm{d}\bar{r}\,\mathrm{d}\overline{\theta} \tag{19b}$$

$$\boldsymbol{Q}_{b}^{i} = \frac{qR^3}{D}\int\int_{\overline{A}} \frac{\sin\theta}{\overline{\varphi}}\phi_{b}^{i}\,\mathrm{d}\bar{r}\,\mathrm{d}\overline{\theta} \tag{19c}$$

The integral notation in Eqs. (18a–f) is defined as

$$I_{\alpha\beta}^{ij(abcd;e,f)} = \int\int_{\overline{A}} \frac{\partial^{a+b}\phi_{\alpha}^{i}(\bar{r},\overline{\theta})}{\partial\bar{r}^{a}\partial\overline{\theta}^{b}}\frac{\partial^{c+d}\phi_{\beta}^{i}(\bar{r},\overline{\theta})}{\partial\bar{r}^{c}\partial\overline{\theta}^{d}}\bar{r}^{e}\bar{h}_{\theta}^{f}\,\mathrm{d}\bar{r}\,\mathrm{d}\overline{\theta} \tag{20}$$

By specifying an external loading parameter qR^3/D, the system of non-homogeneous equations (16) can be solved to yield the response of the helicoidal structure. This system can be solved numerically using a standard numerical solver, such as the IMSL library in Fortran, to obtain the deformation solution.

Detailed derivatives of the energy functional as given in Eq. (15) are presented in Appendix A.

4. Boundary conditions and admissible shape functions

There are four boundaries for the helicoid considered in this manuscript, two for $r =$ constant and another two for $\theta =$ constant. For each boundary, there are four geometric or natural boundary conditions. Due to geometric symmetry of a helicoid for every cycle of 360° along the axis, we have the following geometric boundary conditions when analyzing one-cycle of helicoid. At the two boundaries when $\theta = 0°$ and $\theta = 360°$ which coincide with the x-axis (Figs. 1 and 2), the geometric boundary conditions are

$$u_{\theta} = u_{b} = 0 \tag{21}$$

The displacement component $u_r \neq 0$ applies on these boundaries because the helicoid is subjected to an external loading in the x-direction while $u_{\theta} = u_b = 0$ apply because of symmetry of repeating helicoid for every unit of 360°. For the other two free boundaries where $\bar{r} = 1 - b/R$ (inner boundary) and $\bar{r} = 1$ (outer boundary), there is no geometric boundary conditions as no displacement or rotation is constrained. Unlike the plate and shell analyses, the four natural boundary conditions on the boundary of $r =$ constant involves coupled relations of normal force N_r, tangential force $N_{r\theta}$, shear forces Q_r, bending moment M_r and twisting moment $M_{r\theta}$. Similarly, the other two natural boundary conditions on the boundary of $\theta =$ constant involves coupled relations of N_{θ}, $N_{\theta r}$, Q_{θ}, M_{θ} and $M_{\theta r}$. The exact governing differential equations and natural boundary conditions can be derived using the Euler–Lagrange equation, the Hamitonian principle or the method of variation of energy (Goldenveizer, 1961; Novozhilov, 1964; Leissa, 1973; Rao, 1991) which is not within the scope of this analysis. Coupling of these terms in the natural boundary conditions surfaced due to the presence of the non-linear radius of pretwist $1/R_{r\theta}$. A description on natural boundary conditions of a helicoidal structure can be referred to Goldenveizer (1961) but no explicit expression is available. Fortunately, only the geometric boundary conditions are required using the Ritz principle here. The geometric boundary conditions in Eq. (21) can be imposed to the strain energy and work expressions in Eqs. (10)–(12) as described below.

The geometric boundary conditions in Eq. (21) indicates that the helicoid is not properly supported and will experience a rigid body translation along the x-direction when subject to the distributed loading. Here, we deal with an infinitely long periodic helicoidal structure and the interest is in the relative deformation of helicoid with respect to a reference point, in this case the origin at (0,0,0), which translates in parallel with the rigid body motion. The rigid body mode has been intentionally excluded by setting at the outset the existence of strain energy in Eq. (5) due to the relative deformation of helicoidal structure during bending.

With periodic boundary conditions in Eq. (21) and using the orthogonality of trigonometric functions, it is easy to verify that displacement and stress fields of the periodic helicoidal structure can be expressed in trigonometric series in terms of $\sin\theta$ and $\cos\theta$. Therefore, the two-dimensional shell-like problem can be simplified into a one-dimensional beam-like problem. The more complicated two-dimensional shell-like analysis has been adopted here in order to facilitate generalization of infinitely long helicoidal structure in this paper to a more realistic finite helicoid with non-periodic boundary conditions.

The displacement components $(\bar{u}_r, \bar{u}_\theta, \bar{u}_b)$ at mid-surface of helicoidal structure are approximated by finite series expressed in Eqs. (13a–c). The corresponding admissible shape functions $(\phi_r, \phi_\theta, \phi_b)$ are sets of geometrically compliant two-dimensional polynomials derived such that the geometric boundary conditions are satisfied at the outset. They are composed of the product of a series of simple two-dimensional polynomials $F(\bar{r}, \overline{\theta})$ and boundary-compliant basic functions ϕ_r^b, ϕ_θ^b, ϕ_b^b. The latter are geometric expressions of the helicoid boundary raised to an appropriate basic power in accordance with the corresponding boundary constraints. Accordingly, the admissible shape functions are

$$\sum_{i=1}^{m} \phi_\alpha^i = F(\bar{r}, \overline{\theta})\phi_\alpha^b; \quad F(\bar{r}, \overline{\theta}) = \sum_{q=0}^{p} \sum_{i=0}^{q} \bar{r}^{q-i}\overline{\theta}^i \tag{22a, b}$$

where $\alpha = r$, θ or b. The highest degree of polynomial in the functions is p and it is related to the number of terms m by

$$m = \frac{(p+1)(p+2)}{2} \tag{23}$$

The boundary-compliant basic functions ϕ_r^b, ϕ_θ^b, ϕ_b^b are defined as the product of the equations of continuous piecewise boundary geometries raised to an appropriate basic power that corresponds to the type of boundary constraint. For constraints as given in Eq. (21), the basic functions are

$$\phi_r^b = 1; \quad \phi_\theta^b = \overline{\theta}(\overline{\theta} - 1); \quad \phi_b^b = \overline{\theta}(\overline{\theta} - 1) \tag{24}$$

and, therefore the corresponding admissible shape functions are

$$\sum_{i=1}^{m} \phi_r^i = \sum_{q=0}^{p} \sum_{i=0}^{q} \bar{r}^{q-i}\overline{\theta}^i; \quad \sum_{i=1}^{m} \phi_\theta^i = \overline{\theta}(\overline{\theta} - 1) \sum_{q=0}^{p} \sum_{i=0}^{q} \bar{r}^{q-i}\overline{\theta}^i; \quad \sum_{i=1}^{m} \phi_b^i = \overline{\theta}(\overline{\theta} - 1) \sum_{q=0}^{p} \sum_{i=0}^{q} \bar{r}^{q-i}\overline{\theta}^i \tag{25a–c}$$

5. Results and discussion on non-linear twisting curvature

In many previous dynamic analyses of turbomachinery blade and pretwisted plates, a linearized twisting curvature of $a/R_{r\theta} \approx -\tan\theta_0$ (Leissa et al., 1982, 1984; Leissa and Ewing, 1983; Lee et al., 1984; Liew and Lim, 1994a,b; Liew et al., 1994, 1995; Lim and Liew, 1995a,b) has been adopted. The linearized twisting curvature thus is only valid for a small angle of pretwist. No research has been performed as to what extent the linearized twisting curvature is applicable except the preliminary analyses of Lim (1999a,b). This issue is herewith discussed in detail.

The derivation of non-linear twisting curvature in Eq. (3c) has generalized the conventional linearized twisting curvature $a/R_{r\theta} \approx -\tan\theta_0$ so that a highly pretwisted helicoidal structure can be analyzed. There exist two inherent approximations in assuming $a/R_{r\theta} \approx -\tan\theta_0$ instead of that in Eq. (3c). First, $\theta_0 \approx \tan\theta_0$ and second, $a/R_{r\theta} \approx -\theta_0$ is only valid if $r\varphi \ll 1$. Error in the first assumption is direct as an error of approximately 10% will occur if the angle of pretwist is $\theta_0 = 30°$. To analyze the error due to the second assumption, we have to refer to Fig. 3. In Fig. 3, the relationship of large non-linear twisting curvature

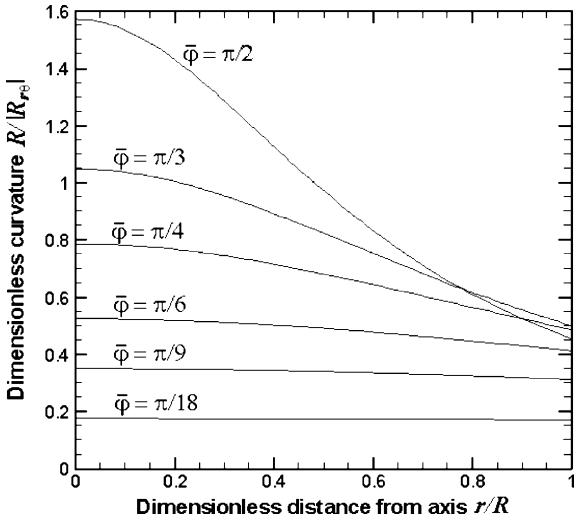

Fig. 3. Large non-linear twisting curvature for constant dimensionless rate of pretwist $\overline{\varphi}$.

$$\frac{R}{|R_{r\theta}|} = \frac{\overline{\varphi}}{1 + \bar{r}^2\overline{\varphi}^2} \tag{26}$$

with respect to the distance from helicoid axis r/R, for constant dimensionless rate of pretwist $\overline{\varphi}$, is presented. Considering a pretwisted surface of constant rate of pretwist $\overline{\varphi}$ $(= R\theta_0/a)$ as shown in Fig. 3, the twisting curvature at a point r/R from the axis would be almost constant $(\approx \overline{\varphi})$ if $\overline{\varphi} \leqslant \pi/18$ rad or 10°. As $\overline{\varphi}$ is dependent on the projected angle θ_0 and a/R, it implies that θ_0 must be remained very small for a short helicoidal structure or a short turbomachinery blade (a small a/R) if a linearized twisting curvature is to be used. On the other hand, θ_0 may be allowed to have a higher value if the a/R ratio for the helicoidal structure or turbomachinery blade is large. Nevertheless, $\overline{\varphi} \leqslant \pi/18$ must be upheld so long as the linearized twisting curvature is used. It is interesting to see in Fig. 3 that the twisting curvature decreases from the axis outwards. It decreases quite linearly for $\overline{\varphi} \approx \pi/9$ rad or 20° and fairly linearly for $\overline{\varphi} \approx \pi/6$ rad or 30°. For $\overline{\varphi} \geqslant \pi/6$, the non-linearity effect becomes very obvious and a non-linear twisting curvature in accordance with Eq. (3c) must be adopted. As shown in Fig. 3, the twisting curvature along the axis $(r/R = 0)$ increases for an increasing $\overline{\varphi}$. However, it is interesting to note that for very high $\overline{\varphi} \geqslant \pi/2$, the twisting curvature on the outer boundary of the helicoid $(r/R = 1)$ is actually smaller than that of a smaller $\overline{\varphi}$. In reality, the twisting curvature decreases sharply and then it approaches a constant value asymptotically when $r/R \to 1$ for a helicoid with a very high $\overline{\varphi}$, given by

$$\lim_{\overline{\varphi}\to\infty} \frac{R}{|R_{r\theta}|} = \frac{1}{\bar{r}^2\overline{\varphi}} \tag{27}$$

In Fig. 4, the relationship of twisting curvature with respect to varying $\overline{\varphi}$ for constant r/R is presented. In this case, the effect of $\overline{\varphi}$ on $R/|R_{r\theta}|$ for a constant r/R can be analyzed. Considering a helix (see Fig. 1) with a constant r/R, the twisting curvature increases when dimensionless rate of pretwist $\overline{\varphi}$ increases from zero initially. As $\overline{\varphi}$ further increases, the twisting curvature reaches a maximum before it starts decreasing. The maximum twisting curvature could be achieved if $\overline{\varphi}$ maintains a particular relationship with respect to r/R. The maximum twisting curvature could be determined by differentiating $R/|R_{r\theta}|$ in Eq. (26) with respect to $\overline{\varphi}$ and setting it to zero, $\mathrm{d}(R/|R_{r\theta}|)/\mathrm{d}\overline{\varphi} = 0$, thus yielding

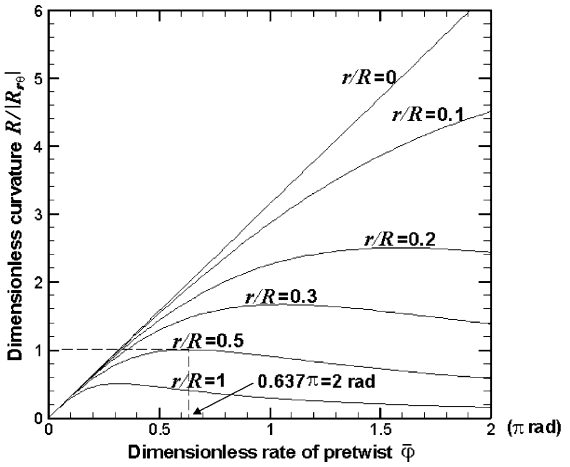

Fig. 4. Large non-linear twisting curvature for constant dimensionless distance r/R.

$$\left.\frac{R}{|R_{r\theta}|}\right|_{\max} = \frac{\overline{\varphi}}{2} = \frac{1}{2\bar{r}} \tag{28}$$

which occurs at $\overline{\varphi} = 1/\bar{r}$. As shown in Fig. 4, for instance, the maximum twisting curvature for $\bar{r} = 0.5$ is $(R/|R_{r\theta}|)_{\max} = 1$ which occurs at $\overline{\varphi} = 2$ rad.

6. Convergence study and numerical examples

As the displacement admissible functions involve finite polynomial series, convergence of numerical solutions has to be established. The convergence of maximum dimensionless bending deflection $\bar{u}_{\max}$ for an infinite helicoid with $v = 0.3$ and $qR^3/D = 1$ is presented in Tables 1 and 2 for two cases of helicoid thickness $h/R = 0.02$ and $h/R = 0.04$, respectively. Various helicoid geometric parameters are considered, ranging from highly pretwisted to slightly pretwisted (increasing a/R) and from slender to wide (increasing b/R). Two components $\bar{u}_\theta$ and $\bar{u}_b$ are tabulated along with the resultant displacement $\bar{u}_{\max} = \sqrt{\bar{u}_r^2 + \bar{u}_\theta^2 + \bar{u}_b^2}$. Values for the third component $\bar{u}_r$ are not presented because $\bar{u}_r$ at maximum bending deflection is a few orders smaller than the other two components and it contributes insignificantly to the maximum resultant displacement $\bar{u}_{\max}$.

In Tables 1 and 2, the number of terms in the series representation in Eqs. (13a–c) are increased steadily. As observed, very good numerical convergence has been achieved and in many cases the error of convergence is less than 1%. Convergence tests were stopped at different values of m when numerical ill-conditioning of matrix appears thus prohibiting accurate numerical solutions be obtained for higher values of m. A number of significant numerical phenomena have also been observed. For a slender helicoid (a small width ratio b/R), numerical instability occurs for a small value of m as compared to a wide helicoid. This is because b/R is a parameter equivalent to the aspect ratio for a rectangular plate. A rectangular plate with a small aspect ratio resembles a beam and in this case the two-dimensional mid-plane of a plate may well be represented as a one-dimensional mid-axis. Thus the plate analysis reduces to the beam analysis. If two-dimensional numerical representation is used to simulate a one-dimensional beam model, numerical instability usually occurs because one of the dimensions is far higher than the other. In Tables 1 and 2, $m = 5$ (21 terms) are included in the displacement admissible functions (13a–c) for $b/R = 0.2$ while $m = 7$ (36 terms) are included in the functions for $b/R = 0.7$.

Table 1
Convergence of maximum dimensionless bending deflection ($\times 10^{-3}$) for an infinite helicoid with $v = 0.3$, $h/R = 0.02$, $qR^3/D = 1$ where $\bar{u}_{\max}$ occurs at $\bar{r} = 1$ and $\theta_0 = \pi/2$ rad or $3\pi/2$ rad

a/R	b/R	p	$\bar{u}_\theta$	$\bar{u}_b$	$\bar{u}_{\max}$
5	0.2	4	0.13909	1.5319	1.5382
		5	0.13970	1.5458	1.5521
	0.3	4	0.092116	0.79004	0.79539
		5	0.093682	0.81727	0.82262
	0.4	4	0.069523	0.51883	0.52347
		5	0.071897	0.55265	0.55731
		6	0.072638	0.55381	0.55855
	0.5	4	0.056761	0.40278	0.40676
		5	0.060022	0.44508	0.44911
		6	0.060095	0.44608	0.45011
	0.6	4	0.051149	0.37948	0.38291
		5	0.055897	0.43509	0.43867
		6	0.056381	0.44139	0.44498
		7	0.056588	0.44297	0.44657
	0.7	4	0.050333	0.40074	0.40389
		5	0.056565	0.46042	0.46389
		6	0.057844	0.47694	0.48044
		7	0.058063	0.47751	0.48103
10	0.2	4	0.47968	5.5653	5.5859
		5	0.48078	5.5939	5.6145
	0.3	4	0.31326	2.5888	2.6077
		5	0.31564	2.6354	2.6543
	0.4	4	0.23107	1.5307	1.5480
		5	0.23452	1.5850	1.6023
		6	0.23633	1.5929	1.6098
	0.5	4	0.18126	1.0300	1.0459
		5	0.18577	1.0935	1.1092
		6	0.18758	1.0942	1.1102
	0.6	4	0.15008	0.79812	0.81214
		5	0.15642	0.88088	0.89468
		6	0.15664	0.88369	0.89754
		7	0.15689	0.88593	0.89979
	0.7	4	0.13253	0.73106	0.74302
		5	0.14169	0.83999	0.85190
		6	0.14292	0.85542	0.86737
		7	0.14343	0.85878	0.87077

Having established the convergence and accuracy of numerical solutions, some numerical examples are presented to study the effects of various geometric parameters on the bending deformation of helicoid. In Figs. 5–8, the effects of width ratio b/R on the maximum resultant bending deformation $\bar{u}_{\max}$ is investigated for helicoid of increasing pretwist (decreasing a/R) and increasing thickness ratio h/R. For a dimensionless rate of pretwist $\overline{\varphi} = \theta_0/(a/R)$ with a fixed periodic helicoid where $\theta_0 = 360°$, we may regard the helicoid as having a low rate of pretwist for a high a/R and vice versa. From Fig. 5, it is observed that $\bar{u}_{\max}$ decreases

Table 2
Convergence of maximum dimensionless bending deflection ($\times 10^{-3}$) for an infinite helicoid with $v = 0.3$, $h/R = 0.04$, $qR^3/D = 1$ where $\bar{u}_{\max}$ occurs at $\bar{r} = 1$ and $\theta_0 = \pi/2$ rad or $3\pi/2$ rad

a/R	b/R	p	$\bar{u}_\theta$	$\bar{u}_b$	$\bar{u}_{\max}$
5	0.2	4	0.54310	5.7570	5.7825
		5	0.54424	5.7716	5.7972
	0.3	4	0.34318	2.6743	2.6962
		5	0.34612	2.7153	2.7373
	0.4	4	0.25682	1.7380	1.7569
		5	0.26251	1.8067	1.8257
		6	0.26492	1.8076	1.8269
	0.5	4	0.20675	1.2803	1.2969
		5	0.21488	1.3667	1.3835
		6	0.21737	1.3685	1.3857
		7	0.21738	1.3690	1.3862
	0.6	4	0.17423	1.0345	1.0490
		5	0.18473	1.1393	1.1541
		6	0.18763	1.1441	1.1593
		7	0.18788	1.1465	1.1618
	0.7	4	0.15570	0.93835	0.95118
		5	0.16957	1.0707	1.0840
		6	0.17055	1.0764	1.0898
		7	0.17106	1.0801	1.0936
10	0.2	4	1.8965	21.663	21.746
		5	1.8992	21.712	21.795
	0.3	4	1.2156	9.5585	9.6355
		5	1.2206	9.6395	9.7165
	0.4	4	0.89075	5.5394	5.6107
		5	0.89929	5.6568	5.7278
		6	0.90582	5.6636	5.7356
	0.5	4	0.69714	3.6336	3.6999
		5	0.70880	3.7717	3.8378
		6	0.71474	3.7895	3.8564
		7	0.71483	3.7981	3.8648
	0.6	4	0.56452	2.5380	2.6002
		5	0.57900	2.6950	2.7566
		6	0.58490	2.7057	2.7682
		7	0.58501	2.7064	2.7690
	0.7	4	0.46966	1.8874	1.9452
		5	0.48798	2.0772	2.1340
		6	0.49460	2.0855	2.1434
		7	0.49514	2.0895	2.1474

sharply for a slender helicoid when b/R is increasing. At a certain b/R, a minimum $\bar{u}_{\max}$ is reached and beyond this point, an increase in b/R causes $\bar{u}_{\max}$ to increase. However, the rate of increase of $\bar{u}_{\max}$ beyond the critical $\bar{u}_{\max}$ is much smaller than the rate of decrease before the critical $\bar{u}_{\max}$. In Figs. 6–8, similar phenomenon is observed except that in some of the cases, a critical $\bar{u}_{\max}$ has not been reached within the range of $0.2 \leqslant b/R \leqslant 0.7$ under investigation. A wider helicoid has higher structural stiffness and as the

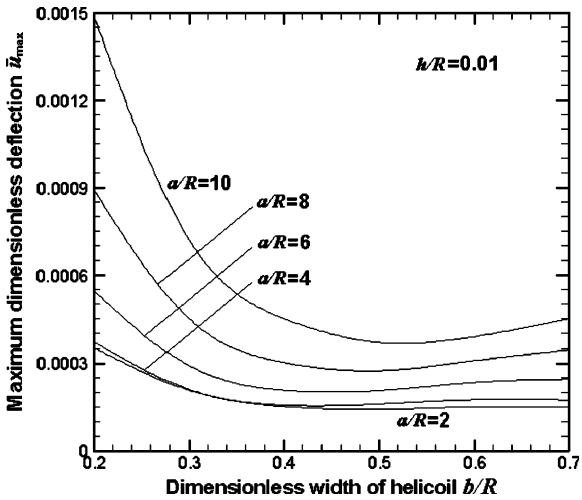

Fig. 5. The effect of dimensionless width on maximum dimensionless deflection for an infinite helicoid with $v = 0.3$, $h/R = 0.01$ and $qR^3/D = 1$.

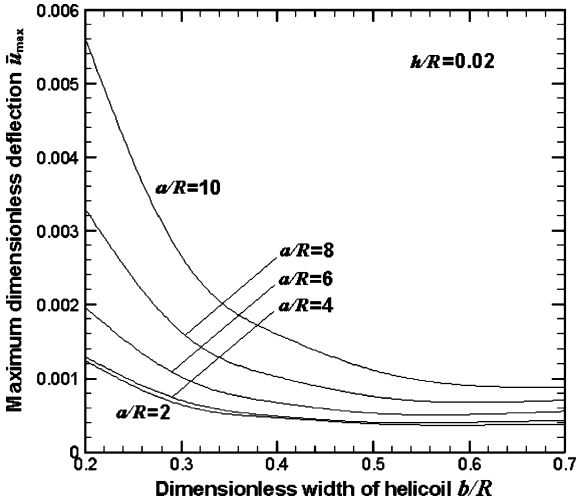

Fig. 6. The effect of dimensionless width on maximum dimensionless deflection for an infinite helicoid with $v = 0.3$, $h/R = 0.02$ and $qR^3/D = 1$.

width ratio increases, the loading is higher because a larger surface of the helicoid is subjected to the pressure loading. From physical point of view, it is the presence of both increasing structural stiffness and increasing pressure loading which determines the existence a critical, minimum $\bar{u}_{max}$.

It is also a common fact in Figs. 5–8 that $\bar{u}_{max}$ decreases with decreasing a/R (or increasing pretwist). As pretwist increases, the rate of decrease of $\bar{u}_{max}$ becomes smaller as the curves are closer apart. This fact is consistent with the understanding that the stiffness of a helicoid increases with pretwist and, therefore, a higher pretwist results in smaller deformation.

The effect of thickness ratio h/R on $\bar{u}_{max}$ cannot be directly observed in Figs. 5–8. At the first glance, an increase in h/R results in higher $\bar{u}_{max}$ and it is contradictory to the common perception that a thicker

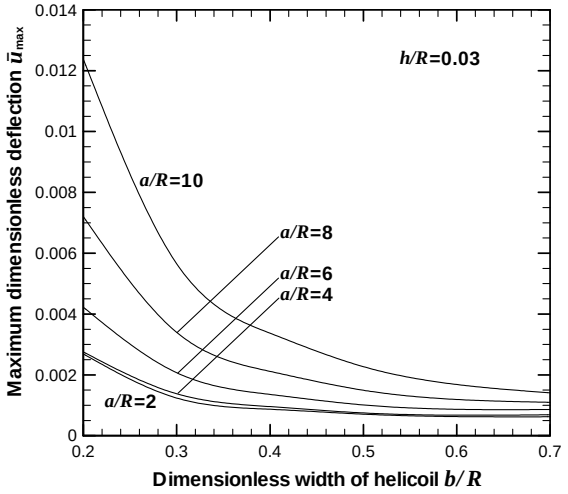

Fig. 7. The effect of dimensionless width on maximum dimensionless deflection for an infinite helicoid with $v = 0.3$, $h/R = 0.03$ and $qR^3/D = 1$.

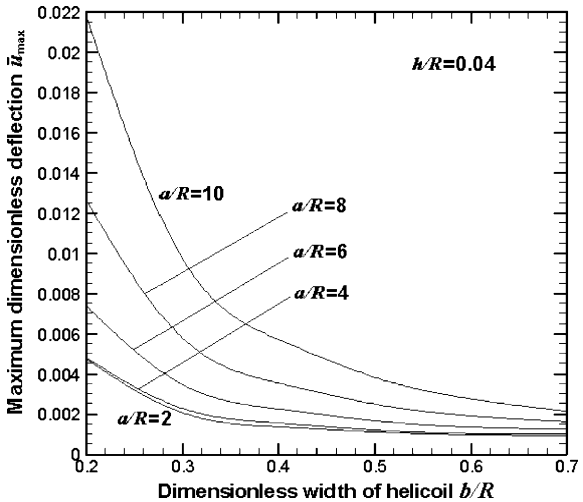

Fig. 8. The effect of dimensionless width on maximum dimensionless deflection for an infinite helicoid with $v = 0.3$, $h/R = 0.04$ and $qR^3/D = 1$.

structure has higher stiffness and thus a smaller deformation. The reason for this inconsistency is very simple. The loadings for all the cases in Figs. 5–8 are different. In all cases, the loading parameter is set at $qR^3/D = 1$. Since the flexural rigidity $D = Eh^3/12(1 - v^2)$ depends on thickness, the loading parameter is, in fact, $q'(R/h)^3$ where $q' = 12(1 - v^2)q/E$. As a result, a n times increase in h/R while maintaining loading at $q'(R/h)^3 = 1$ induces an increase of loading parameter of n^3 times. In this case, the helicoid in Fig. 6 has a thickness ratio of double of that of Fig. 5 but it has a loading eight times higher. Comparing the maximum deflection $\bar{u}_{max}$, it has only increased by less than four times. In conclusion, a double-increase of thickness and an octagonal-increase of loading resulting in less than four times increase in deflection do not contradict the law of physics. The same reasoning applies to a comparison of results in Figs. 6 and 7 and Figs. 7

and 8. Comparing Figs. 6 and 7, the thickness ratio increases by 1.5 times while the loading increases by $1.5^3 = 3.375$ times. Meanwhile, $\bar{u}_{\max}$ increases by approximately 2.2 times.

The deformation modes for a unit ($\theta_0 = 360°$) of infinite helicoids are presented in Figs. 9–11, respectively, for a slender helicoid, a wide helicoid and a helicoid with a smaller pretwist. Undeformed and deformed modes are presented for comparison and clarity. The magnitudes of dimensionless orthogonal deformation components $\bar{u}_r$, $\bar{u}_\theta$, $\bar{u}_b$ and their resultant $\bar{u} = \sqrt{\bar{u}_r^2 + \bar{u}_\theta^2 + \bar{u}_b^2}$ are also presented for the inner (closer to the axis) and outer (further to the axis) boundaries, respectively. Major contribution of resultant deformation comes from $\bar{u}_b$ and this is particularly obvious for the outer boundary. In all cases, the maximum resultant $\bar{u}_{\max}$ always occurs at $\theta_0 = \pi/2$ rad and $3\pi/2$ rad because these lines on the helicoidal surface are normal to the loading direction.

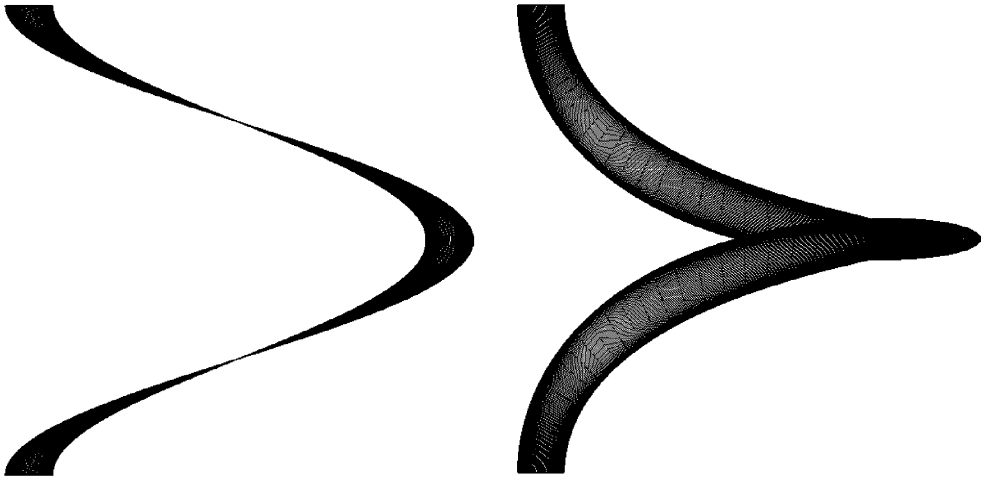

(a) Undeformed structure

(b) Deformed structure

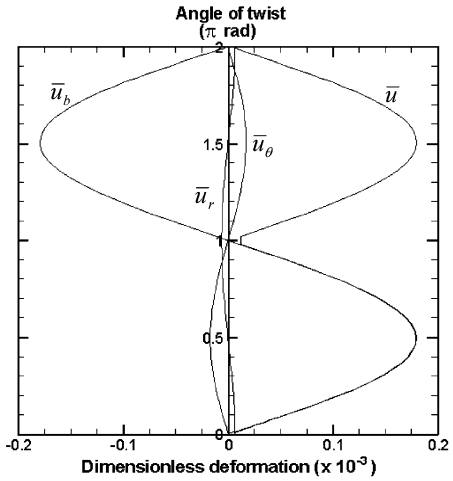

(c) Deformation of inner boundary

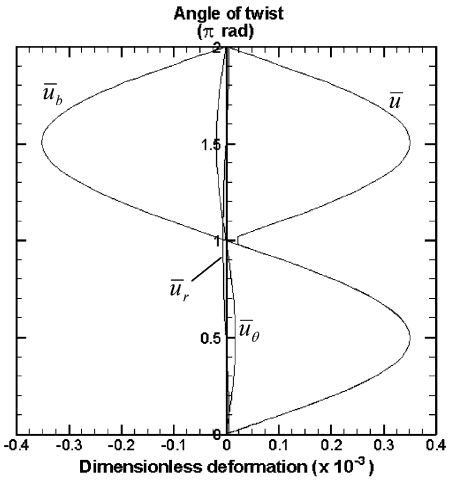

(d) Deformation of outer boundary

Fig. 9. Deformation of an infinite helicoid with $v = 0.3$, $a/R = 2$, $b/R = 0.2$, $h/R = 0.01$, $\theta_0 = 360°$ and $qR^3/D = 1$.

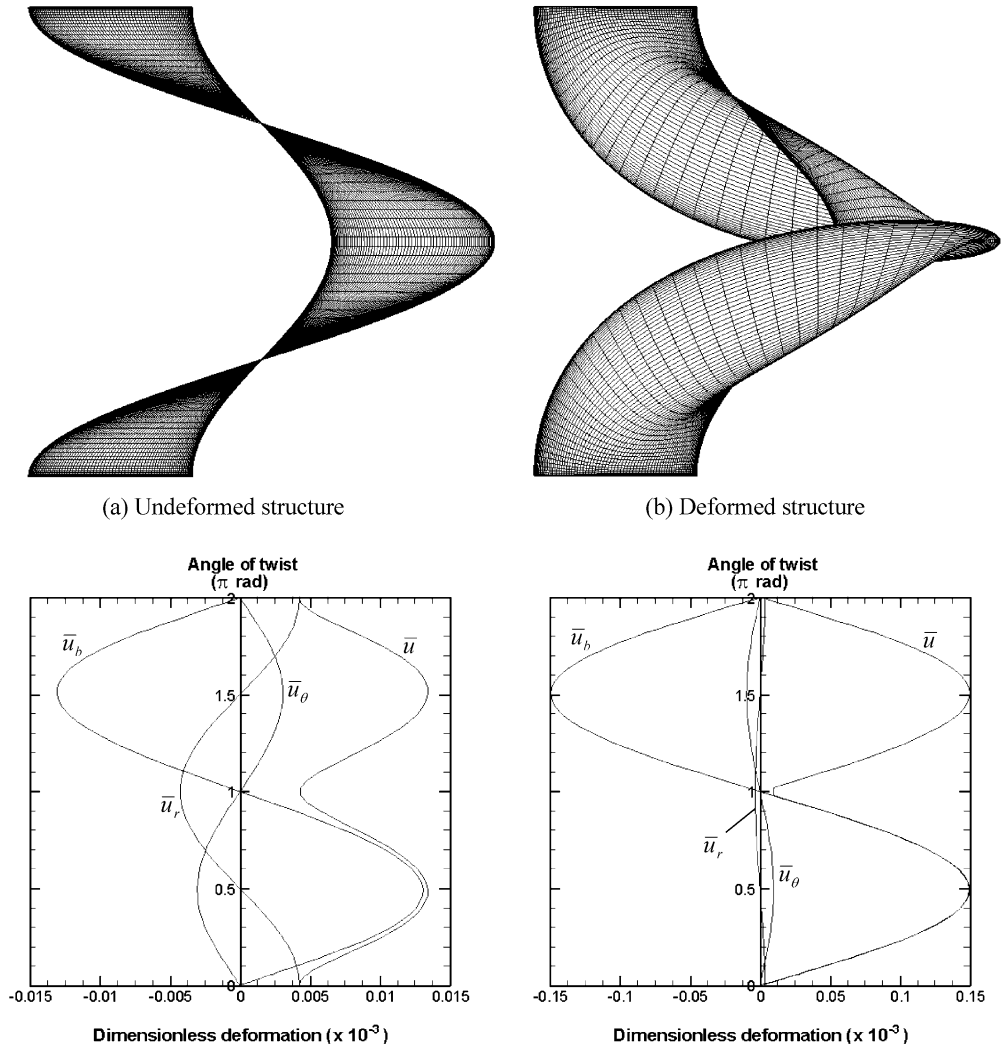

(a) Undeformed structure (b) Deformed structure

(c) Deformation of inner boundary (d) Deformation of outer boundary

Fig. 10. Deformation of an infinite helicoid with $v = 0.3$, $a/R = 2$, $b/R = 0.7$, $h/R = 0.01$, $\theta_0 = 360°$ and $qR^3/D = 1$.

It is also observed that the outer boundary deforms higher than the inner boundary. As discussed in Fig. 3, the magnitude of twisting curvature decreases from the helicoid axis outwards along the radial direction. Because the local stiffness is dependent on the magnitude of twisting curvature, the inner boundary would have smaller deformation than the outer boundary as its twisting curvature, and thus its local stiffness, is higher. For instance, the magnitude of $\bar{u}$ increases from the inner boundary to the outer boundary by approximately two times in Figs. 9 and 11 while in Fig. 10, the increase is approximately 10 times.

It is interesting to note that $\bar{u}_r$, $\bar{u}_\theta$, $\bar{u}_b$ and $\bar{u}$ are periodic with respect to one-cycle or 360° of helicoid. This is expected for an infinitely long helicoid because the deformation pattern repeats itself for every cycle of helicoid along the axis due to symmetry in geometry and pressure loading. It is also noted that $\bar{u}_\theta$ is always 180° out-of-phase with respect to the $\bar{u}_b$ for the inner boundary but they are both in-phase for the outer boundary. For both the inner and outer boundaries, $\bar{u}_r$ is always 90° out-of-phase with respect to the other two components.

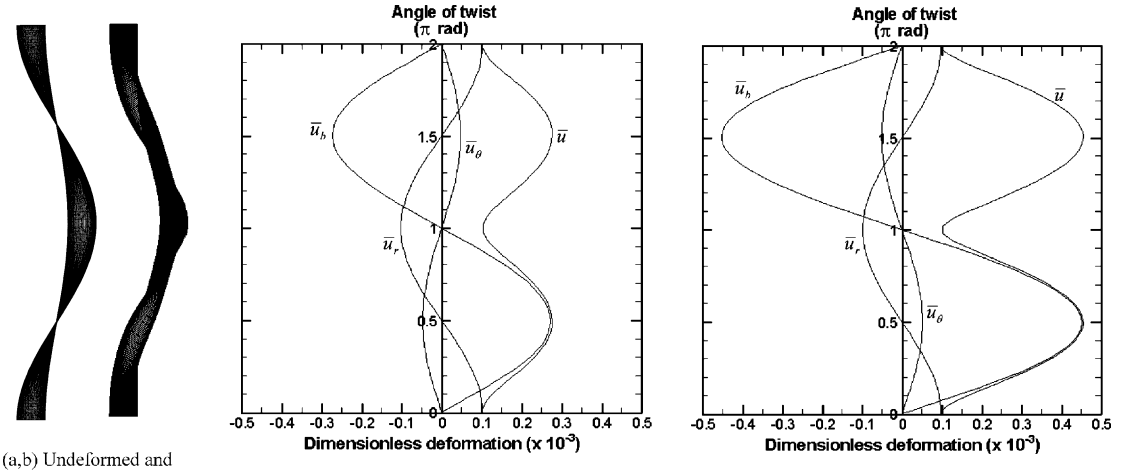

Fig. 11. Deformation of an infinite helicoid with $v = 0.3$, $a/R = 10$, $b/R = 0.7$, $h/R = 0.01$, $\theta_0 = 360°$ and $qR^3/D = 1$.

Comparing Fig. 10 with Fig. 9, the corresponding dimensionless deformation components are of similar patterns because a steady, constant pressure loading is considered in these examples. A decrease in structural stiffness or an increase in pressure loading will anticipate an increase in deformation amplitude. For instance, the overall stiffness of a slender helicoid ($b/R = 0.2$) in Fig. 9 is smaller than the overall stiffness of a wider helicoid ($b/R = 0.7$) in Fig. 10. Therefore, the magnitude of deformation in Fig. 9 is higher than the corresponding values in Fig. 10. By adjusting the width of the helicoid without changing the magnitude of pressure loading distribution on the helicoidal structure, it is possible to simulate and determine the overall stiffness of a helicoidal structure. It is also possible to adopt a varying thickness helicoid $h(r, \theta)$ so that the stiffness at any single point on the domain of helicoid could be characterized accordingly.

7. Concluding remarks

A new helicoidal model with a large non-linear pretwist based on a natural orthogonal coordinate system has been established for the bending analysis of helicoidal structures subject to external pressure loading. The paper also draws a guideline on the extent of applicability of the linearized twisting curvature model conventionally adopted in analysis of pretwisted plates. Employing the new model, the strain energy stored in a distorted helicoid and the pressure work of external pressure loading normal to the helicoid axis have been derived. By integrating the internal strain energy and external pressure work over the helicoidal domain via the Ritz principle, a non-homogeneous system of equations has been obtained.

The effects of non-linear twisting curvature have been discussed at length. Significant numerical solutions for structural responses such as deformation components and resultant, effects of width and thickness of helicoid on bending have been analyzed and discussed. Among the important conclusions are:

- the linearized twisting curvature model is only valid for a small rate of pretwist, $\overline{\varphi} \leqslant \pi/18$ rad;
- the non-linear twisting curvature decreases from the axis outwards and it approaches a constant value, given by Eq. (27), asymptotically;
- for a helix with varying rate of pretwist, the maximum dimensionless non-linear twisting curvature is given by half of the dimensionless rate of pretwist which is in turn given by the reciprocal of the dimensionless radial distance, as given by Eq. (28);

- the maximum dimensionless deflection $\bar{u}_{\max}$ decreases with respect to increasing width ratio and there exists a critical $\bar{u}_{\max}$;
- $\bar{u}_{\max}$ decreases for a helicoid with increasing rate of pretwist;
- $\bar{u}_{\max}$ always occurs at $\theta_0 = \pi/2$ rad and $3\pi/2$ rad at the outer boundary ($\bar{r} = 1$) on the helicoidal surface and these lines are normal to the loading direction;
- for the inner boundary of a helicoid, $\bar{u}_\theta$ is always 180° out-of-phase with respect to $\bar{u}_b$ but they are both in-phase for the outer boundary, while, for both the inner and outer boundaries, $\bar{u}_r$ is always 90° out-of-phase with respect to the other two components; and
- the outer boundary of a helicoid has larger deformation comparing to the inner boundary because its local stiffness is smaller.

The analysis can be extended to other areas of interest such as turbomachinery blades, drilling structures, motors in MEMS and also DNA biomechanics.

Acknowledgements

The work described in this paper was fully supported by grants from City University of Hong Kong [Project No. 7001186 (BC)] and Research Grant Council of the Hong Kong Special Administrative Region [Project No. CityU 1036/01E]. The detailed comments of reviewers are also gratefully acknowledged.

Appendix A

The derivative of the strain energy components in Eq. (15) can be derived as

$$\begin{aligned}\frac{\partial U_s}{\partial C_r^i} &= \frac{6R^2D}{h^2}\int\!\!\int_{\bar{A}}\left\{2\theta_0\bar{h}_\theta\frac{\partial\phi_r^i}{\partial\bar{r}}\frac{\partial\bar{u}_r}{\partial\bar{r}}+\frac{2\bar{r}}{\bar{h}_\theta^2}\phi_r^i\frac{\partial\bar{u}_\theta}{\partial\overline{\theta}}+\frac{2\theta_0\bar{r}^2}{\bar{h}_\theta^3}\phi_r^i\bar{u}_r+2\nu\left[\frac{\partial\phi_r^i}{\partial\bar{r}}\frac{\partial\bar{u}_\theta}{\partial\overline{\theta}}+\frac{\theta_0\bar{r}}{\bar{h}_\theta}\left(\phi_r^i\frac{\partial\bar{u}_r}{\partial\bar{r}}+\frac{\partial\phi_r^i}{\partial\bar{r}}\bar{u}_r\right)\right]\right.\\ &\quad\left.+(1-\nu)\left[\frac{\partial\phi_r^i}{\partial\overline{\theta}}\frac{\partial\bar{u}_\theta}{\partial\bar{r}}-\frac{\bar{r}}{\bar{h}_\theta^2}\frac{\partial\phi_r^i}{\partial\overline{\theta}}\bar{u}_\theta+\frac{1}{\theta_0\bar{h}_\theta}\frac{\partial\phi_r^i}{\partial\overline{\theta}}\frac{\partial\bar{u}_r}{\partial\overline{\theta}}-\frac{2}{\overline{\varphi}\bar{h}_\theta^2}\frac{\partial\phi_r^i}{\partial\overline{\theta}}\bar{u}_b\right]\right\}\mathrm{d}\bar{r}\,\mathrm{d}\overline{\theta}\\ &= \frac{6R^2D}{h^2}\sum_{j=1}^{m}\left\{2\theta_0C_r^jI_{rr}^{ij(1010;0,1)}+2C_\theta^jI_{r\theta}^{ij(0001;1,-2)}+2\theta_0C_r^jI_{rr}^{ij(0000;2,-3)}\right.\\ &\quad+2\nu\left[C_\theta^jI_{r\theta}^{ij(1001;0,0)}+\theta_0C_r^j\left(I_{rr}^{ij(0010;1,-1)}+I_{rr}^{ij(1010;1,-1)}\right)\right]+(1-\nu)\left[C_\theta^jI_{r\theta}^{ij(0110;0,0)}-C_\theta^jI_{r\theta}^{ij(0100;1,-2)}\right.\\ &\quad\left.\left.+\frac{1}{\theta_0}C_r^jI_{rr}^{ij(0101;0,-1)}-\frac{2}{\overline{\varphi}}C_b^jI_{rb}^{ij(0100;0,-2)}\right]\right\}\end{aligned}\tag{A.1}$$

$$\begin{aligned}\frac{\partial U_s}{\partial C_\theta^i} &= \frac{6R^2D}{h^2}\int\!\!\int_{\bar{A}}\left\{\frac{2}{\bar{h}_\theta}\frac{\partial\phi_\theta^i}{\partial\overline{\theta}}\frac{\partial\bar{u}_\theta}{\partial\overline{\theta}}+\frac{2\bar{r}}{\bar{h}_\theta^2}\frac{\partial\phi_\theta^i}{\partial\overline{\theta}}\bar{u}_r+2\nu\frac{\partial\phi_\theta^i}{\partial\overline{\theta}}\frac{\partial\bar{u}_r}{\partial\bar{r}}+(1-\nu)\left[\theta_0\bar{h}_\theta\frac{\partial\phi_\theta^i}{\partial\bar{r}}\frac{\partial\bar{u}_\theta}{\partial\bar{r}}-\frac{\theta_0\bar{r}}{\bar{h}_\theta}\left(\phi_\theta^i\frac{\partial\bar{u}_\theta}{\partial\bar{r}}+\frac{\partial\phi_\theta^i}{\partial\bar{r}}\bar{u}_\theta\right)\right.\right.\\ &\quad\left.\left.+\frac{\partial\phi_\theta^i}{\partial\bar{r}}\frac{\partial\bar{u}_r}{\partial\overline{\theta}}-\frac{2\theta_0}{\overline{\varphi}\bar{h}_\theta}\frac{\partial\phi_\theta^i}{\partial\bar{r}}\bar{u}_b+\frac{\theta_0\bar{r}^2}{\bar{h}_\theta^3}\phi_\theta^i\bar{u}_\theta-\frac{\bar{r}}{\bar{h}_\theta^2}\phi_\theta^i\frac{\partial\bar{u}_r}{\partial\overline{\theta}}+\frac{2\theta_0\bar{r}}{\overline{\varphi}\bar{h}_\theta^3}\phi_\theta^i\bar{u}_b\right]\right\}\mathrm{d}\bar{r}\,\mathrm{d}\overline{\theta}\\ &= \frac{6R^2D}{h^2}\sum_{j=1}^{m}\left\{2C_\theta^jI_{\theta\theta}^{ij(0101;0,-1)}+2C_r^jI_{\theta r}^{ij(0100;1,-2)}+2\nu C_r^jI_{\theta r}^{ij(0110;0,0)}+(1-\nu)\left[\theta_0C_\theta^jI_{\theta\theta}^{ij(1010;0,1)}\right.\right.\\ &\quad-\theta_0C_\theta^j\left(I_{\theta\theta}^{ij(0010;1,-1)}+I_{\theta\theta}^{ij(1000;1,-1)}\right)+C_r^jI_{\theta r}^{ij(1001;0,0)}-\frac{2\theta_0}{\overline{\varphi}}C_b^jI_{\theta b}^{ij(1000;0,-1)}+\theta_0C_\theta^jI_{\theta\theta}^{ij(0000;2,-3)}\\ &\quad\left.\left.-C_r^jI_{\theta r}^{ij(0001;1,-2)}+\frac{2\theta_0}{\overline{\varphi}}C_b^jI_{\theta b}^{ij(0000;1,-3)}\right]\right\}\end{aligned}\tag{A.2}$$

$$\frac{\partial U_{\mathrm{s}}}{\partial C_b^i} = \frac{6R^2D}{h^2}\int\int_{\bar{A}}\left\{(1-\nu)\left[\frac{-2\theta_0}{\overline{\varphi}\bar{h}_\theta}\phi_b^i\frac{\partial\bar{u}_\theta}{\partial\bar{r}} + \frac{2\theta_0\bar{r}}{\overline{\varphi}\bar{h}_\theta^3}\phi_b^i\bar{u}_\theta - \frac{2}{\overline{\varphi}\bar{h}_\theta^2}\phi_b^i\frac{\partial\bar{u}_r}{\partial\bar{\theta}} + \frac{4\theta_0}{\overline{\varphi}^2\bar{h}_\theta^3}\phi_b^i\bar{u}_b\right]\right\}\mathrm{d}\bar{r}\,\mathrm{d}\bar{\theta}$$
$$= \frac{6R^2D}{h^2}\frac{2(1-\nu)}{\overline{\varphi}}\sum_{j=1}^{m}\left[-\theta_0 C_\theta^j I_{b\theta}^{ij(0010;0,-1)} + \theta_0 C_\theta^j I_{b\theta}^{ij(0000;1,-3)} - C_r^j I_{br}^{ij(0001;0,-2)} + \frac{2\theta_0}{\overline{\varphi}}C_b^j I_{bb}^{ij(0000;0,-3)}\right] \tag{A.3}$$

$$\frac{\partial U_{\mathrm{b}}}{\partial C_r^i} = \frac{D}{2}\int\int_{\bar{A}}\left\{\frac{5-3\nu}{\theta_0\overline{\varphi}^2\bar{h}_\theta^5}\frac{\partial\phi_r^i}{\partial\bar{\theta}}\frac{\partial\bar{u}_r}{\partial\bar{\theta}} + \frac{(3-5\nu)\bar{r}}{\overline{\varphi}^2\bar{h}_\theta^6}\frac{\partial\phi_r^i}{\partial\bar{\theta}}\bar{u}_\theta - \frac{3-5\nu}{\overline{\varphi}^2\bar{h}_\theta^4}\frac{\partial\phi_r^i}{\partial\bar{\theta}}\frac{\partial\bar{u}_\theta}{\partial\bar{r}} + \frac{(3-\nu)\bar{r}}{\overline{\varphi}\bar{h}_\theta^4}\frac{\partial\phi_r^i}{\partial\bar{\theta}}\frac{\partial\bar{u}_b}{\partial\bar{r}}\right.$$
$$- \frac{1-3\nu}{\overline{\varphi}\bar{h}_\theta^2}\frac{\partial\phi_r^i}{\partial\bar{\theta}}\frac{\partial^2\bar{u}_b}{\partial\bar{r}^2} + \frac{3-\nu}{\overline{\theta}_0^2\overline{\varphi}\bar{h}_\theta^4}\frac{\partial\phi_r^i}{\partial\bar{\theta}}\frac{\partial^2\bar{u}_b}{\partial\bar{\theta}^2} + \frac{4(1-\nu)}{\overline{\varphi}\bar{h}_\theta}\left[\frac{1}{\bar{h}_\theta}\frac{\partial\phi_r^i}{\partial\bar{r}}\frac{\partial^2\bar{u}_b}{\partial\bar{r}\partial\bar{\theta}} - \frac{\bar{r}}{\bar{h}_\theta^3}\phi_r^i\frac{\partial^2\bar{u}_b}{\partial\bar{r}\partial\bar{\theta}} - \frac{\bar{r}}{\bar{h}_\theta^3}\frac{\partial\phi_r^i}{\partial\bar{r}}\frac{\partial\bar{u}_b}{\partial\bar{\theta}}\right.$$
$$\left.\left.+ \frac{\bar{r}^2}{\bar{h}_\theta^5}\phi_r^i\frac{\partial\bar{u}_b}{\partial\bar{\theta}} + \frac{\theta_0}{\overline{\varphi}\bar{h}_\theta^2}\frac{\partial\phi_r^i}{\partial\bar{r}}\frac{\partial\bar{u}_r}{\partial\bar{r}} + \frac{1}{\overline{\varphi}\bar{h}_\theta^3}\frac{\partial\phi_r^i}{\partial\bar{r}}\frac{\partial\bar{u}_\theta}{\partial\bar{\theta}} - \frac{\theta_0\bar{r}}{\overline{\varphi}\bar{h}_\theta^4}\left(\phi_r^i\frac{\partial\bar{u}_r}{\partial\bar{r}} + \frac{\partial\phi_r^i}{\partial\bar{r}}\bar{u}_r\right) - \frac{\bar{r}}{\overline{\varphi}\bar{h}_\theta^5}\phi_r^i\frac{\partial\bar{u}_\theta}{\partial\bar{\theta}} + \frac{\theta_0\bar{r}^2}{\overline{\varphi}\bar{h}_\theta^6}\phi_r^i\bar{u}_r\right]\right\}\mathrm{d}\bar{r}\,\mathrm{d}\bar{\theta}$$
$$= \frac{D}{2\overline{\varphi}}\sum_{j=1}^{m}\left\{\frac{5-3\nu}{\theta_0\overline{\varphi}}C_r^j\mathrm{I}_{rr}^{ij(0101;0,-5)} + \frac{3-5\nu}{\overline{\varphi}}C_\theta^j I_{r\theta}^{ij(0100;1,-6)} - \frac{3-5\nu}{\overline{\varphi}}C_\theta^j I_{r\theta}^{ij(0110;0,-4)} + (3-\nu)C_b^j I_{rb}^{ij(0110;1,-4)}\right.$$
$$- (1-3\nu)C_b^j I_{rb}^{ij(0120;0,-2)} + \frac{3-\nu}{\theta_0^2}C_b^j I_{rb}^{ij(0102;0,-4)} + 4(1-\nu)\left[C_b^j I_{rb}^{ij(1011;0,-2)} - C_b^j I_{rb}^{ij(0011;1,-4)}\right.$$
$$- C_b^j I_{rb}^{ij(1001;1,-4)} + C_b^j I_{rb}^{ij(0001;2,-6)} + \frac{\theta_0}{\overline{\varphi}}C_r^j I_{rr}^{ij(1010;0,-3)} + \frac{1}{\overline{\varphi}}C_\theta^j I_{r\theta}^{ij(1001;0,-4)}$$
$$\left.\left.- \frac{\theta_0}{\overline{\varphi}}C_r^j\left(I_{rr}^{ij(0010;1,-5)} + I_{rr}^{ij(1000;1,-5)}\right) - \frac{1}{\overline{\varphi}}C_\theta^j I_{r\theta}^{ij(0001;1,-6)} + \frac{\theta_0}{\overline{\varphi}}C_r^j I_{rr}^{ij(0000;2,-7)}\right]\right\} \tag{A.4}$$

$$\frac{\partial U_{\mathrm{b}}}{\partial C_\theta^i} = \frac{D}{2}\int\int_{\bar{A}}\left\{\frac{(3-5\nu)\bar{r}}{\overline{\varphi}^2\bar{h}_\theta^6}\phi_\theta^i\frac{\partial\bar{u}_r}{\partial\bar{\theta}} + \frac{3-5\nu}{\overline{\varphi}^2\bar{h}_\theta^4}\frac{\partial\phi_r^i}{\partial\bar{r}}\frac{\partial\bar{u}_r}{\partial\bar{\theta}} - \frac{(5-3\nu)\theta_0\bar{r}^2}{\overline{\varphi}^2\bar{h}_\theta^7}\phi_\theta^i\bar{u}_\theta - \frac{(5-3\nu)\theta_0\bar{r}}{\overline{\varphi}^2\bar{h}_\theta^5}\left(\phi_\theta^i\frac{\partial\bar{u}_\theta}{\partial\bar{r}} + \frac{\partial\phi_\theta^i}{\partial\bar{r}}\bar{u}_\theta\right)\right.$$
$$+ \frac{(1-3\nu)\overline{\theta}_0\bar{r}^2}{\overline{\varphi}\bar{h}_\theta^5}\phi_\theta^i\frac{\partial\bar{u}_b}{\partial\bar{r}} - \frac{(3-\nu)\overline{\theta}_0\bar{r}}{\overline{\varphi}\bar{h}_\theta^3}\phi_\theta^i\frac{\partial^2\bar{u}_b}{\partial\bar{r}^2} + \frac{(1-3\nu)\bar{r}}{\overline{\theta}_0\overline{\varphi}\bar{h}_\theta^5}\phi_\theta^i\frac{\partial^2\bar{u}_b}{\partial\bar{\theta}^2} + \frac{(5-3\nu)\theta_0}{\overline{\varphi}^2\bar{h}_\theta^3}\frac{\partial\phi_\theta^i}{\partial\bar{r}}\frac{\partial\bar{u}_\theta}{\partial\bar{r}}$$
$$- \frac{(1-3\nu)\theta_0\bar{r}}{\overline{\varphi}\bar{h}_\theta^3}\frac{\partial\phi_\theta^i}{\partial\bar{r}}\frac{\partial\bar{u}_b}{\partial\bar{r}} + \frac{(3-\nu)\theta_0}{\overline{\varphi}\bar{h}_\theta}\frac{\partial\phi_\theta^i}{\partial\bar{r}}\frac{\partial^2\bar{u}_b}{\partial\bar{r}^2} - \frac{1-3\nu}{\theta_0\overline{\varphi}\bar{h}_\theta^3}\frac{\partial\phi_\theta^i}{\partial\bar{r}}\frac{\partial^2\bar{u}_b}{\partial\bar{\theta}^2} + \frac{4(1-\nu)}{\overline{\varphi}\bar{h}_\theta}\left[\frac{1}{\theta_0\bar{h}_\theta^2}\frac{\partial\phi_\theta^i}{\partial\bar{\theta}}\frac{\partial^2\bar{u}_\theta}{\partial\bar{r}\partial\bar{\theta}}\right.$$
$$\left.\left.- \frac{\bar{r}}{\theta_0\bar{h}_\theta^4}\frac{\partial\phi_\theta^i}{\partial\bar{\theta}}\frac{\partial\bar{u}_b}{\partial\bar{\theta}} + \frac{1}{\overline{\varphi}\bar{h}_\theta^3}\frac{\partial\phi_\theta^i}{\partial\bar{\theta}}\frac{\partial\bar{u}_r}{\partial\bar{r}} + \frac{1}{\theta_0\overline{\varphi}\bar{h}_\theta^4}\frac{\partial\phi_\theta^i}{\partial\bar{\theta}}\frac{\partial\bar{u}_\theta}{\partial\bar{\theta}} - \frac{\bar{r}}{\overline{\varphi}\bar{h}_\theta^5}\frac{\partial\phi_\theta^i}{\partial\bar{\theta}}\bar{u}_r\right]\right\}\mathrm{d}\bar{r}\,\mathrm{d}\bar{\theta}$$
$$= \frac{D}{2\overline{\varphi}}\sum_{j=1}^{m}\left\{\frac{3-5\nu}{\overline{\varphi}}C_r^j I_{\theta r}^{ij(0001;1,-6)} - \frac{3-5\nu}{\overline{\varphi}}C_r^j I_{\theta r}^{ij(1001;0,-4)} + \frac{(5-3\nu)\theta_0}{\overline{\varphi}}C_\theta^j I_{\theta\theta}^{ij(0000;2,-7)}\right.$$
$$- \frac{(5-3\nu)\theta_0}{\overline{\varphi}}C_\theta^j\left(I_{\theta\theta}^{ij(0010;1,-5)} + I_{\theta\theta}^{ij(1000;1,-5)}\right) + (1-3\nu)\theta_0 C_b^j I_{\theta b}^{ij(0010;2,-5)}$$
$$- (3-\nu)\theta_0 C_b^j I_{\theta b}^{ij(0020;1,-3)} + \frac{1-3\nu}{\theta_0}C_b^j I_{\theta b}^{ij(0002;1,-5)} + \frac{(5-3\nu)\theta_0}{\overline{\varphi}}C_\theta^j I_{\theta\theta}^{ij(1010;0,-3)}$$
$$+ 4(1-\nu)\left[\frac{1}{\theta_0}C_b^j I_{\theta b}^{ij(1011;0,-2)} - \frac{1}{\theta_0}C_b^j I_{\theta b}^{ij(0101;1,-5)} + \frac{1}{\overline{\varphi}}C_r^j I_{\theta r}^{ij(0110;0,-4)}\right.$$
$$\left.\left.- \frac{1}{\theta_0\overline{\varphi}}C_\theta^j I_{r\theta}^{ij(0101;0,-5)} - \frac{1}{\overline{\varphi}}C_r^j I_{\theta r}^{ij(0100;1,-6)}\right]\right\} \tag{A.5}$$

$$
\begin{aligned}
\frac{\partial U_{\mathrm{b}}}{\partial C_b^i} = \frac{D}{2}\int\int_{\bar{A}} \Bigg\{ & \frac{(3-\nu)\bar{r}}{\overline{\varphi}\bar{h}_\theta^4}\frac{\partial\phi_b^i}{\partial\bar{r}}\frac{\partial\bar{u}_r}{\partial\overline{\theta}} - \frac{1-3\nu}{\overline{\varphi}\bar{h}_\theta^2}\frac{\partial^2\phi_b^i}{\partial\bar{r}^2}\frac{\partial\bar{u}_r}{\partial\overline{\theta}} + \frac{3-\nu}{\theta_0\overline{\varphi}\bar{h}_\theta^4}\frac{\partial^2\phi_b^i}{\partial\overline{\theta}^2}\frac{\partial\bar{u}_r}{\partial\overline{\theta}} + \frac{(1-3\nu)\theta_0\bar{r}^2}{\overline{\varphi}\bar{h}_\theta^5}\frac{\partial\phi_b^i}{\partial\bar{r}}\bar{u}_\theta \\
& - \frac{(3-\nu)\overline{\theta}_0\bar{r}}{\overline{\varphi}\bar{h}_\theta^3}\frac{\partial^2\phi_b^i}{\partial\bar{r}^2}\bar{u}_\theta + \frac{(1-3\nu)\bar{r}}{\theta_0\overline{\varphi}\bar{h}_\theta^5}\frac{\partial^2\phi_b^i}{\partial\overline{\theta}^2}\bar{u}_\theta - \frac{(1-3\nu)\theta_0\bar{r}}{\overline{\varphi}\bar{h}_\theta^3}\frac{\partial\phi_b^i}{\partial\bar{r}}\frac{\partial\bar{u}_\theta}{\partial\bar{r}} + \frac{(3-\nu)\overline{\theta}_0}{\overline{\varphi}\bar{h}_\theta}\frac{\partial^2\phi_b^i}{\partial\bar{r}^2}\frac{\partial\bar{u}_\theta}{\partial\bar{r}} \\
& - \frac{1-3\nu}{\theta_0\overline{\varphi}\bar{h}_\theta^3}\frac{\partial\phi_b^i}{\partial\overline{\theta}^2}\frac{\partial\bar{u}_\theta}{\partial\bar{r}} - \frac{2\theta_0\bar{r}^2}{\bar{h}_\theta^3}\frac{\partial\phi_b^i}{\partial\bar{r}}\frac{\partial\bar{u}_b}{\partial\bar{r}} + \frac{2\nu\theta_0\bar{r}}{\bar{h}_\theta}\left(\frac{\partial\phi_b^i}{\partial\bar{r}}\frac{\partial^2\bar{u}_b}{\partial\bar{r}^2} + \frac{\partial^2\phi_b^i}{\partial\bar{r}^2}\frac{\partial\bar{u}_b}{\partial\bar{r}}\right) \\
& + \frac{2\bar{r}}{\theta_0\bar{h}_\theta^3}\left(\frac{\partial\phi_b^i}{\partial\bar{r}}\frac{\partial^2\bar{u}_b}{\partial\overline{\theta}^2} + \frac{\partial^2\phi_b^i}{\partial\overline{\theta}^2}\frac{\partial\bar{u}_b}{\partial\bar{r}}\right) + 2\theta_0\bar{h}_\theta\frac{\partial^2\phi_b^i}{\partial\bar{r}^2}\frac{\partial^2\bar{u}_b}{\partial\bar{r}^2} + \frac{2\nu}{\theta_0\bar{h}_\theta}\left(\frac{\partial^2\phi_b^i}{\partial\bar{r}^2}\frac{\partial^2\bar{u}_b}{\partial\overline{\theta}^2} + \frac{\partial^2\phi_b^i}{\partial\overline{\theta}^2}\frac{\partial^2\bar{u}_b}{\partial\bar{r}^2}\right) \\
& - \frac{2}{\theta_0^3\bar{h}_\theta^3}\frac{\partial^2\phi_b^i}{\partial\overline{\theta}^2}\frac{\partial^2\bar{u}_b}{\partial\overline{\theta}^2} + \frac{4(1-\nu)}{\bar{h}_\theta}\left[\frac{1}{\theta_0}\frac{\partial^2\phi_b^i}{\partial\bar{r}\partial\overline{\theta}}\frac{\partial^2\bar{u}_b}{\partial\bar{r}\partial\overline{\theta}} - \frac{\bar{r}}{\theta_0\bar{h}_\theta^2}\left(\frac{\partial\phi_b^i}{\partial\overline{\theta}}\frac{\partial^2\bar{u}_b}{\partial\bar{r}\partial\overline{\theta}} + \frac{\partial^2\phi_b^i}{\partial\bar{r}\partial\overline{\theta}}\frac{\partial\bar{u}_b}{\partial\overline{\theta}}\right) + \frac{1}{\overline{\varphi}\bar{h}_\theta}\frac{\partial^2\phi_b^i}{\partial\bar{r}\partial\overline{\theta}}\frac{\partial\bar{u}_r}{\partial\bar{r}}\right. \\
& \left. + \frac{1}{\theta_0\overline{\varphi}\bar{h}_\theta^2}\frac{\partial^2\phi_b^i}{\partial\bar{r}\partial\overline{\theta}}\frac{\partial\bar{u}_\theta}{\partial\overline{\theta}} - \frac{\bar{r}}{\overline{\varphi}\bar{h}_\theta^3}\frac{\partial^2\phi_b^i}{\partial\bar{r}\partial\overline{\theta}}\bar{u}_r + \frac{\bar{r}^2}{\theta_0\bar{h}_\theta^4}\frac{\partial\phi_b^i}{\partial\overline{\theta}}\frac{\partial\bar{u}_b}{\partial\overline{\theta}} - \frac{\bar{r}}{\theta_0\overline{\varphi}\bar{h}_\theta^4}\frac{\partial\phi_b^i}{\partial\overline{\theta}}\frac{\partial\bar{u}_\theta}{\partial\overline{\theta}} + \frac{\bar{r}^2}{\overline{\varphi}\bar{h}_\theta^5}\frac{\partial\phi_b^i}{\partial\overline{\theta}}\bar{u}_r\right]\Bigg\}\mathrm{d}\bar{r}\,\mathrm{d}\overline{\theta} \\
= \frac{D}{2}\sum_{j=1}^{m}\Bigg\{ & \frac{3-\nu}{\overline{\varphi}}C_r^j I_{br}^{ij(1001;1,-4)} - \frac{1-3\nu}{\overline{\varphi}}C_r^j I_{br}^{ij(2001;0,-2)} + \frac{3-\nu}{\theta_0^2\overline{\varphi}}C_r^j I_{br}^{ij(0201;0,-4)} + \frac{(1-3\nu)\theta_0}{\overline{\varphi}}C_\theta^j I_{b\theta}^{ij(1000;2,-5)} \\
& - \frac{(3-\nu)\theta_0}{\overline{\varphi}}C_\theta^j I_{b\theta}^{ij(2000;1,-3)} + \frac{1-3\nu}{\theta_0\overline{\varphi}}C_\theta^j I_{b\theta}^{ij(0200;1,-5)} - \frac{(1-3\nu)\theta_0}{\overline{\varphi}}C_\theta^j I_{b\theta}^{ij(1010;1,-3)} \\
& - \frac{(3-\nu)\theta_0}{\overline{\varphi}}C_\theta^j I_{b\theta}^{ij(2010;0,-1)} + \frac{1-3\nu}{\theta_0\overline{\varphi}}C_\theta^j I_{b\theta}^{ij(0210;0,-3)} + 2\theta_0 C_b^j I_{bb}^{ij(1010;2,-3)} \\
& + 2\nu\theta_0 C_b^j\left(I_{bb}^{ij(1020;1,-1)} + I_{bb}^{ij(2010;1,-1)}\right) + \frac{2}{\theta_0}C_b^j\left(I_{bb}^{ij(1002;1,-3)} + I_{bb}^{ij(0210;1,-3)}\right) + 2\theta_0 C_b^j I_{bb}^{ij(2020;0,1)} \\
& + \frac{2\nu}{\theta_0}C_b^j\left(I_{bb}^{ij(2002;0,-1)} + I_{bb}^{ij(0220;0,-1)}\right) + \frac{2}{\theta_0^3}C_b^j I_{bb}^{ij(0202;0,-3)} \\
& + 4(1-\nu)\left[\frac{1}{\theta_0}C_b^j I_{bb}^{ij(1111;0,-1)} - \frac{1}{\theta_0}\left(C_b^j I_{bb}^{ij(0111;1,-3)} + C_b^j I_{bb}^{ij(1101;1,-3)}\right) + \frac{1}{\overline{\varphi}}C_r^j I_{br}^{ij(1110;0,-2)}\right. \\
& + \frac{1}{\theta_0\overline{\varphi}}C_\theta^j I_{b\theta}^{ij(1101;0,-3)} - \frac{1}{\overline{\varphi}}C_r^j I_{br}^{ij(1100;1,-4)} + \frac{1}{\theta_0}C_b^j I_{bb}^{ij(0101;2,-5)} - \frac{1}{\overline{\varphi}}C_r^j I_{br}^{ij(0110;1,-4)} - \frac{1}{\theta_0\overline{\varphi}}C_\theta^j I_{b\theta}^{ij(0101;1,-5)} \\
& \left. - \frac{1}{\overline{\varphi}}C_r^j I_{br}^{ij(0100;2,-6)}\right]\Bigg\} \qquad \text{(A.6)}
\end{aligned}
$$

References

Challamel, N., 2000. Rock destruction effect on the stability of a drilling structure. J. Sound Vib. 233 (2), 235–254.

Christoforou, A.P., Yigit, A.S., 1997. Dynamic modelling of drillstrings with borehole interactions. J. Sound Vib. 206 (2), 243–260.

Goldenveizer, A.L., 1961. Theory of Thin Shells. Pergamon Press, New York.

Kielb, R.E., Leissa, A.W., MacBain, J.C., 1985. Vibrations of twisted cantilevered plates—A comparison of theoretical results. Int. J. Numer. Meth. Eng. 21, 1365–1380.

Knowles, J.K., Reissner, E., 1959. Torsion and extension of helicoidal shells. Quart. Appl. Math. 17, 409–422.

Lee, J.K., Leissa, A.W., Wang, A.J., 1984. Vibrations of blades with variable thickness and curvature by shell theory. J. Eng. Gas Turb. Power 106 (1), 11–16.

Leissa, A.W., 1973. Vibration of shells. NASA SP-288.

Leissa, A.W., 1980. Vibrations of turbine engine blades by shell analysis. Shock Vib. Digest 12 (11), 3–10.

Leissa, A.W., 1981. Vibrational aspects of rotating turbomachinery blades. Appl. Mech. Rev. 34 (5), 629–635.
Leissa, A.W., Ewing, M.S., 1983. Comparison of beam and shell theories for the vibrations of thin turbomachinery blades. J. Eng. Power 105 (2), 383–392.
Leissa, A.W., Lee, J.K., Wang, A.J., 1982. Rotating blade vibration analysis using shells. J. Eng. Power 104 (2), 296–302.
Leissa, A.W., MacBain, J.C., Kielb, R.E., 1984. Vibrations of twisted cantilevered plates—Summary of previous and current studies. J. Sound Vib. 96 (2), 159–173.
Leung, A.Y.T., 1991. Exact shape functions for helix elements. FE Ana. Design. 9 (1), 23–32.
Leung, A.Y.T., Chan, J.K.W., 1997. On the love strain form of naturally curved and twisted rods. Thin-Walled Struct. 28 (3–4), 253–267.
Liew, K.M., Lim, C.W., 1994a. A global continuum Ritz formulation for flexural vibration of pretwisted trapezoidal plates with one edge built in. Comp. Meth. Appl. Mech. Eng. 114 (1–2), 233–247.
Liew, K.M., Lim, C.W., 1994b. Vibratory characteristics of cantilevered rectangular shallow shells of variable thickness. AIAA J. 32 (2), 387–396.
Liew, K.M., Lim, C.W., Ong, L.S., 1994. Vibration of pretwisted cantilever shallow conical shells. Int. J. Solids Struct. 31 (18), 2463–2476.
Liew, K.M., Lim, M.K., Lim, C.W., Li, D.B., Zhang, Y.R., 1995. Effects of initial twist and thickness variation on the vibration behaviour of shallow conical shells. J. Sound Vib. 180 (2), 271–296.
Lim, C.W., 1999a. Investigating the limit of turbomachinery blade modelling with linear pretwist. In: Ewing, M.S., Leissa, A.W. (Eds.), 2nd Int. Symp. Vib. Continuous Sys., 12–16 July, Switzerland, pp. 33–35.
Lim, C.W., 1999b. Vibration of turbomachinery blades with non-linear twisting curvature. In: Wang, C.M., Lee, K.H., Ang, K.K. (Eds.), APCOM '99, 15–17 December, Singapore, pp. 493–498.
Lim, C.W., Liew, K.M., 1995a. Vibration of pretwisted cantilever trapezoidal symmetric laminates. Acta Mech. 111 (3–4), 193–208.
Lim, C.W., Liew, K.M., 1995b. The vibration behaviour of shallow conical shells by a global Ritz formulation. Eng. Struct. 17 (1), 63–70.
MacBain, J.C., Kielb, R.E., Leissa, A.W., 1985. Vibration of twisted cantilevered plates—Experimental investigation. J. Eng. Gas Turb. Power. 107, 187–196.
Mallett, R.L., Wan, F.Y.M., 1971. Spirally sinusoidal stress distributions in elastic helicoidal shells. J. Appl. Math. Phys. 22, 1029–1043.
Mallett, R.L., Wan, F.Y.M., 1973. The static–geometric duality and a staggered mesh scheme in the numerical solution of some shell problems. Stud. Appl. Math. 52, 21–38.
Maunder, L., Reissner, E., 1957. Pure bending of pretwisted rectangular plates. J. Mech. Phys. Solids 5, 261–266.
Mockensturm, E.M., Mote, C.D., 2001. Free response of twisted plates with fixed support separation. J. Vib Acous. 123, 175–180.
Novozhilov, V.V., 1964. The Theory of Thin Elastic Shells. P. Noordhoff, Groningen, The Netherlands.
O'Mathuna, D., 1963. Rotationally symmetric deformations in helicoidal shells. J. Math. Phys. 42, 85–111.
Rao, J.S., 1973. Natural frequencies of turbine blading—A survey. Shock Vib. Digest 5 (10), 3–16.
Rao, J.S., 1977. Turbine blading excitation and vibration. Shock Vib. Digest 9 (3), 15–22.
Rao, J.S., 1980. Turbomachine blade vibration. Shock Vib. Digest 12 (2), 19–26.
Rao, J.S., 1983. Turbomachine blade vibration. Shock Vib. Digest 15 (5), 3–9.
Rao, J.S., 1987. Turbomachine blade vibration. Shock Vib. Digest 19 (5), 3–10.
Rao, J.S., 1991. Turbomachine Blade Vibration. John Wiley & Sons, Singapore.
Rao, J.S., Carnegie, W., 1970. Solution of the equations of motion of couple-bending torsion vibrations of turbine blades by the method of Ritz–Galerkin. Int. J. Mech. Sci. 12 (10), 875–882.
Reissner, E., 1954. On finite bending and twisting of circular ring sector plates and shallow helicoidal shells. Quart. Appl. Math. 11, 473–483.
Reissner, E., 1959. On twisting and stretching of helicoidal shells. In: Proc. IUTAM Symp. on Thin Shell Theory, Amsterdam, 1960, pp. 434–466.
Reissner, E., Wan, F.Y.M., 1968. On axial extension and torsion of helicoidal shells. J. Math. Phys. 47 (1), 1–31.
Reissner, E., Wan, F.Y.M., 1971. On stretching, twisting, pure bending and flexure of pretwisted elastic plates. Int. J. Solids Struct. 7, 625–637.
Selvam, S.V.M., Sujatha, C., 1995. Twist drill deformation and optimum drill geometry. Computers Struct. 57 (5), 903–914.
Tsuiji, T., Takagi, K., Sueoka, T., 1994a. Free vibrations of curved and twisted thin plates (Fundamental theory). Trans. JSME 60 (C), 4073–4078 (in Japanese).
Tsuiji, T., Takagi, K., Sueoka, T., 1994b. Free vibrations of curved and twisted thin plates (Analytical and experimental results). Trans. JSME 60 (C), 4079–4084 (in Japanese).
Walker, K.P., 1978. Vibrations of cambered helicoidal fan blades. J. Sound Vib. 59 (1), 35–57.
Wan, F.Y.M., 1967. A class of unsymmetric stress distributions in helicoidal shells. Quart. Appl. Math. 24, 374–379.
Wan, F.Y.M., 1968. Pure bending of shallow helicoidal shells. Trans. ASME J. Appl. Mech. 35, 387–392.

Wan, F.Y.M., 1969a. The side force problem for shallow helicoidal shells. Trans. ASME J. Appl. Mech. 36, 292–295.
Wan, F.Y.M., 1969b. St. Venant flexure of pretwisted rectangular plates. Int. J. Eng. Sci. 7, 351–360.
Wan, F.Y.M., 1970. Rotationally symmetric shearing and bending of helicoidal shells. Stud. Appl. Math. 49 (4), 351–369.
Wan, F.Y.M., 1990. Finite axial extension and torsion of elastic helicoidal shells. In: Wong, R. (Ed.), Asymptotic and Computational Analysis. Marcel Dekker, New York, pp. 491–516.
Young, E.C., 1993. Vector and Tensor Analysis. Marcel Dekker, New York, pp. 102–126.